JOURNAL OF GUIDANCE, CONTROL, AND DYNAMICS
Vol. 45, No. 3, March 2022

Robust Control Study for Tethered Payload Transportation Using Multiple Quadrotors

Longhao Qian* and Hugh H. T. Liu†
University of Toronto, North York, Ontario M3H 5T6, Canada

https://doi.org/10.2514/1.G006173

A novel robust path-following flight controller for multiple quadrotors carrying a slung payload is proposed. The payload is manipulated by a group of quadrotors with cables so that every agent shares the payload weight. The system is decomposed into the payload subsystem and the quadrotor attitude subsystems. The controller is hierarchical. The outer loop is a robust path-following controller that stabilizes the payload subsystem. An uncertainty and disturbance estimator is designed to estimate and eliminate the disturbances. The inner loop is an attitude tracker implemented on each quadrotor that follows the target attitude generated by the outer-loop controller. The overall stability of the complete system is shown using the Lyapunov method. Simulations and flight demonstrations show that the controller can stabilize the slung load according to the given path command under exogenous disturbances.

Nomenclature

a_j, $\boldsymbol{D}$, $\boldsymbol{E}_j$	=	weighting parameter and matrices for payload control distribution
$\boldsymbol{B}_j$	=	auxiliary matrix relating the horizontal speed $\boldsymbol{v}_j$ to the cable tip speed $\dot{\boldsymbol{L}}_j$
$\boldsymbol{C}$, $\boldsymbol{M}$	=	Coriolis and inertial matrices of the equations of motion
$\boldsymbol{e}_1, \boldsymbol{e}_2, \boldsymbol{e}_3$	=	unit vectors: $\boldsymbol{e}_1 = [1,0,0]^T$, $\boldsymbol{e}_2 = [0,1,0]^T$, and $\boldsymbol{e}_3 = [0,0,1]^T$
$\boldsymbol{e}_{p,i}$, $\boldsymbol{e}_{v,i}$, $\boldsymbol{e}_r$	=	position, velocity, and attitude error of the payload, respectively, m, m/s, rad
$\boldsymbol{F}$, $\boldsymbol{G}$, $\boldsymbol{\Delta}$	=	actuation, gravitational, and disturbance force terms of equations of motion
$\boldsymbol{f}_{L,j}$, f_j	=	propeller lift of the jth quadrotor expressed in $\mathcal{F}_\mathcal{I}$ and its magnitude, N
$\boldsymbol{g}_I$, g	=	gravitational acceleration vector in $\mathcal{F}_\mathcal{I}$ and its magnitude, m/s^2
$\boldsymbol{J}_p$, $\boldsymbol{J}$	=	moment of inertia of the payload and the quadrotor, respectively, kg · m^2
$\boldsymbol{L}_j$, l	=	cable vector in $\mathcal{F}_\mathcal{I}$ and its magnitude, m
m_p, m_j	=	mass of the payload and the jth quadrotor, kg
N	=	number of quadrotors
$\boldsymbol{n}_i$, $\boldsymbol{p}_i$	=	directional vector and the starting point of the ith segment of the path
$\boldsymbol{R}_{\mathrm{AB}}$	=	rotation matrix from frame A to frame B
$\boldsymbol{r}_j$, $\boldsymbol{v}_j$	=	x and y component of $\boldsymbol{L}_j$ and its time derivative, m, m/s
$\boldsymbol{t}_j$	=	vector from O_P to O_{Tj} in $\mathcal{F}_\mathcal{P}$, i.e., cable anchor position, m
$\boldsymbol{v}_{d,i}$	=	reference speed vector, m/s
$\boldsymbol{v}_p$, $\boldsymbol{x}_p$	=	velocity and position of the payload in the $\mathcal{F}_\mathcal{I}$, m/s
$\boldsymbol{\Delta}_j$, $\boldsymbol{\Delta}_{\parallel,j}$, $\boldsymbol{\Delta}_{\perp,j}$	=	disturbance force on each quadrotor and its components that are parallel and perpendicular to $\boldsymbol{L}_j$, N
$\boldsymbol{\Delta}_t$, $\boldsymbol{\Delta}_r$	=	disturbance force and torque on the payload, N
$\boldsymbol{\tau}_j$	=	torque on each quadrotor, N · m
ϕ, θ, ψ	=	roll, pitch, and yaw angle of the payload receptively, deg
$\boldsymbol{\omega}_p$, $\boldsymbol{\omega}_j$	=	angular velocity of the payload and the jth quadrotor, rad/s
$\mathbf{1}$, $\mathbf{0}$	=	identity matrix and zero matrix of appropriate size, respectively

I. Introduction

QUADROTORS have been seen in a variety of industrial applications, such as surveillance [1] and fire monitoring [2]. Although limited in terms of lifting capability and range, rotorcraft such as quadrotors and helicopters have been used to conduct autonomous transport of slung payloads [3–6]. A field mission was demonstrated by the Kaman K-MAX in Afghanistan [7]. Recently, automatic package delivery systems have also been implemented by Klausen et al. [8] and Geng and Langelaan [9] with commercial drones and cable suspended payloads.

If the payload is tethered to the vehicle via cables, the system is in a slung payload configuration. The main purpose of using the slung payload configuration together with a group of cooperative rotorcraft is to increase the payload capacity. Although heavy lifting missions could be done by specialized vehicles such as the Mi-26 [10] and UH-60 helicopter [5], they are not always available and the cost of operation can be high. Alternatively, using a group of small-sized autonomous rotorcraft in coordination to share a heavy payload has promising potential, and an example is the Boeing Lift! Project [11]. Compared with using robot manipulators, the slung payload configuration is structurally simple and low cost and, therefore, has been extensively studied in literature [12–15]. Traditionally, the slung-load transportation problem requires pilots to fly the helicopters in coordination. However, the task becomes a cooperative flight control problem when autonomous rotorcraft such as quadrotors are used. The technical challenges then lie in the quadrotor-payload stabilization and path-following control. Successful control development could result in precise manipulation of payloads and reduced pilot workload.

The state-of-the-art solution for the coordinated flight control problem can be divided into two main groups: the formation priority (FP) design and the load priority (LP) design. The FP design focuses on maintaining the formation of the vehicles and relies on the cable as a distance constraint to place the payload at the desired position. The cable forces are usually treated as external forces to be compensated [3,4,8]. The Udwadia–Kalaba method is a common approach to obtain the cable tension for force compensation [8]. Dhiman et al. used the pictorial description and a force cone to remap the load control force into a formation trajectory [16]. Rastgoftar and Atkins

Received 2 May 2021; revision received 30 August 2021; accepted for publication 3 September 2021; published online 23 December 2021.

*Ph.D. Candidate, Institute for Aerospace Studies, 4925 Dufferin Street; longhao.qian@mail.utoront.ca.

†Professor, Institute for Aerospace Studies, 4925 Dufferin Street; liu@utias.utoronto.ca. Associate Fellow AIAA.

studied a paradigm (CALM) with the continuum deformation approach to transport the slung load with collision avoidance guarantees [17]. Other types of FP designs such as the passivity-based control by Meissen et al. [18] and the leader–follower scheme by Gassner et al. [19] have also been investigated.

On the other hand, the LP design treats the slung-load system as a complete multibody system and uses linear/nonlinear control techniques to develop a control strategy. The cable forces are then treated as internal forces as a result of length constraint such as the dual-lift system with RMAX helicopters [20] and aerial cable-drive robot system developed by UPenn's GRASP lab [21]. The LP designs attract more attention than the FP designs because they can manipulate the payload precisely and provide deeper insights into such multibody systems. Goodarzi and Lee provided a hierarchical controller based on the linearized multibody slung-load system, and tested the controller in experiments [22]. Wu and Sreenath proposed a control algorithm by using the pseudo-inverse of the control matrix to obtain the reference lift of each quadrotor [23]. An important work by Lee provided a geometric controller for rigid-body slung-load trajectory tracking under disturbances [24]. The disturbances were estimated and compensated by an adaptive law. The flatness methodology and adaptive method were also adopted by Nair et al. to design a slung platform-ball stabilization controller with three quadrotors [25]. Kotaru et al. proposed a differential flatness based method to control a payload while modeling the cables as point masses connected by rigid links [26].

To mitigate the effect of exogenous disturbances, a variety of robust control methods, such as adaptive control [24], sliding mode control [27], and active disturbance rejection control (ADRC), [6] are used. Among these potential candidates, the ADRC design paradigm produces reasonable performance for slung-load systems. The key step is to treat the estimated disturbances as an extended state and design the corresponding error dynamics. The transient property of the estimator can be set so that the estimator injects much less perturbations into the system than the adaptive control design. Compared with sliding mode control, ADRC does not require a high-gain feedback. A special type of ADRC paradigm called the uncertainty and disturbance estimator (UDE) method [28] was investigated in the context of the slung-load systems [6]. It relies on a low-pass filter together with the system model to estimate the disturbances. It captures both the constant and the low-frequency components of the disturbances without introducing large variations into the transient states and is a promising candidate for cooperative slung-load control.

A scalable nonlinear cooperative controller for multiple quadrotors carrying a slung payload was developed in Ref. [12] based on Kane's method and Lyapunov direct method. In this work, the position error and the attitude error of the payload are converted into virtual lift commands. The quadrotors then rotate in the corresponding directions to manipulate the slung load. In addition, a UDE-based robust controller was developed for a single quadrotor carrying a slung payload to facilitate path-following control under exogenous turbulence [6]. This paper combines the previous work [6,12] by extending the UDE concept into the multi-UAV slung-load system to design an LP control law and performing experiments in hardware. The main contributions are thus threefold. First, a full nonlinear controller is introduced and shown to be asymptotically stable (AS). Second, following the UDE design paradigm, an estimator with low-pass properties is introduced to measure the disturbances on the system. The overall virtual control force is fulfilled by an attitude tracker on each quadrotor to point the lift vector in the target direction. Third, the control effectiveness is verified in both simulations and indoor experiments. The controller is able to stabilize the slung load in the presence of disturbances in the form of unknown payload mass distribution.

The remainder of this paper is structured in the following manner: Sec. II provides the problem formulation and the dynamic modeling. Section III presents the controller design. Section IV contains the stability analysis. Sections V and VI demonstrate the performance of the proposed method in simulations and experiments. Finally, Sec. VII contains the research conclusions.

II. Problem Formulation

A. Mathematical Preliminaries

Let $\|\boldsymbol{v}\| = \sqrt{\boldsymbol{v}^T\boldsymbol{v}}$ be the norm of vector $\boldsymbol{v} \in \mathbb{R}^{N\times 1}$. Let $\boldsymbol{M} \in \mathbb{R}^{N\times N}$ be a square matrix, and $\|\boldsymbol{M}\|$ denotes its matrix 2-norm. Let $\boldsymbol{\phi} \in \mathbb{R}^{3\times 1} = [\phi_1 \quad \phi_2 \quad \phi_3]^T$, and $\boldsymbol{\phi}^\times \in \mathbb{R}^{3\times 3}$ is defined as a matrix mapping to a skew-symmetric matrix, i.e., $\boldsymbol{\phi}^\times = -(\boldsymbol{\phi}^\times)^T$. This is also known as the cross-product mapping or Lie algebra. Its inverse mapping to convert a skew symmetric 3-by-3 matrix $\boldsymbol{M}$ is denoted as $\boldsymbol{M}^\vee = [-M_{23} \quad M_{13} \quad -M_{12}]^T \in \mathbb{R}^{3\times 1}$. The coordinate of a vector $\boldsymbol{x}$ in frame A is denoted as $\boldsymbol{x}_A \in \mathbb{R}^{3\times 1}$. The rotation matrix between frame A and frame B is denoted as $\boldsymbol{R}_{\mathrm{AB}} \in SO(3)$. $\boldsymbol{R}_{\mathrm{AB}}\boldsymbol{R}_{BA} = \boldsymbol{R}_{\mathrm{AB}}\boldsymbol{R}_{\mathrm{AB}}^T = \mathbf{1}$. $\boldsymbol{x}_A = \boldsymbol{R}_{\mathrm{AB}}\boldsymbol{x}_B$. Subscript $()_{xy}$ is defined as the x and y component of a vector $\boldsymbol{a} \in \mathbb{R}^{3\times 1}$, i.e., $\boldsymbol{a}_{xy} = [a_1 \quad a_2]^T$.

B. Reference Frames and System States

The geometry of the problem is captured by Fig. 1. A slung payload is lifted by N quadrotors labeled as $j = 1, \ldots, N$. All cables are of the same length of $l \in \mathbb{R}$. $\boldsymbol{\mathcal{F}}_{\mathcal{I}} = \{\mathrm{O}_{\boldsymbol{I}}, \boldsymbol{I}_x, \boldsymbol{I}_y, \boldsymbol{I}_z\}$ is a world fixed north-east-down frame. $\boldsymbol{\mathcal{F}}_{\mathcal{P}} = \{\mathrm{O}_P, \boldsymbol{P}_x, \boldsymbol{P}_y, \boldsymbol{P}_z\}$ is a body-fixed frame on the payload. The rotation matrix between $\boldsymbol{\mathcal{F}}_{\mathcal{I}}$ and $\boldsymbol{\mathcal{F}}_{\mathcal{P}}$ is denoted as $\boldsymbol{R}_{IP}$. $\mathrm{O_P}$ is at the center of mass (CM) of the payload. $\boldsymbol{\mathcal{F}}_{\mathcal{T}_{\mathcal{J}}} = \{\mathrm{O}_{T_j}, \boldsymbol{T}_{x,j}, \boldsymbol{T}_{y,j}, \boldsymbol{T}_{z,j}\}$ is an auxiliary frame with its origin $\mathrm{O_{T_j}}$ fixed at the cable attachment point on the payload that only translates with the payload, i.e., $\boldsymbol{R}_{T_j I} \equiv \mathbf{1}$. The body-fixed frame on the jth quadrotor is $\boldsymbol{\mathcal{F}}_{\mathcal{J}} = \{\mathrm{O}_j, \boldsymbol{j}_x, \boldsymbol{j}_y, \boldsymbol{j}_z\}$. The rotation matrix between $\boldsymbol{\mathcal{F}}_{\mathcal{J}}$ and $\boldsymbol{\mathcal{F}}_{\mathcal{I}}$ is $\boldsymbol{R}_{Ij}$. Each cable is assumed attached to the CM of the quadrotors, so their attitude dynamics are decoupled from the rest of the system. Hence, we define the attitude subsystem corresponding to the jth quadrotor as Σ_j. The rest of the system, including the quadrotor translation dynamics and the payload rigid-body dynamics, is denoted by Σ_p. Σ_p is essentially a rigid body connected with several point masses. The vector from O_P to O_{T_j} is $\boldsymbol{t}_j \in \mathbb{R}^{3\times 1}$, i.e., the cable attachment offset. Note that $\boldsymbol{L}_j$ overlays the cable between the payload and the jth quadrotor. $\boldsymbol{r}_j \in \mathbb{R}^{2\times 1}$ is the projection of $\boldsymbol{L}_j$ onto the x and y plane of $\boldsymbol{\mathcal{F}}_{\mathcal{T}_{\mathcal{J}}}$. The cable has a fixed length, so $\boldsymbol{r}_j$ is sufficient to describe the motion of the quadrotor relative to the payload. A set $\mathcal{X}_p = \{\boldsymbol{x}_p, \boldsymbol{R}_{IP}, \boldsymbol{r}_1, \ldots, \boldsymbol{r}_N, \boldsymbol{v}_p, \boldsymbol{\omega}_p, \boldsymbol{v}_1, \ldots, \boldsymbol{v}_N\}$ is used to denote the state of Σ_p. The set $\mathcal{X}_j = \{\boldsymbol{R}_{Ij}, \boldsymbol{\omega}_j\}$ is used to denote the state of Σ_j. The set $\mathcal{X} = \{\mathcal{X}_p, \mathcal{X}_1, \ldots, \mathcal{X}_N\}$ is used to define the state of the complete system. An auxiliary matrix $\boldsymbol{B}_j \in \mathbb{R}^{3\times 2}$ relating $\boldsymbol{v}_j$ to the tip velocity of the cable, i.e., $\dot{\boldsymbol{L}}_j$, is

$$\boldsymbol{L}_j = \begin{bmatrix} \boldsymbol{r}_j \\ -\sqrt{l^2 - \boldsymbol{r}_j^T\boldsymbol{r}_j} \end{bmatrix}; \quad \boldsymbol{B}_j\boldsymbol{v}_j = \dot{\boldsymbol{L}}_j; \quad \boldsymbol{B}_j = \begin{bmatrix} \mathbf{1}_{2\times 2} \\ \frac{\boldsymbol{r}_j^T}{\sqrt{l^2 - \boldsymbol{r}_j^T\boldsymbol{r}_j}} \end{bmatrix} \tag{1}$$

According to Fig. 1, the positive z direction of $\boldsymbol{\mathcal{F}}_{\mathcal{T}_{\mathcal{J}}}$ points downward so the z component of $\boldsymbol{L}_j$ is negative by definition.

C. Equations of Motion

The equations of motion (EOM) are adopted from our previous work [12] listed as follows:

$$\Sigma_p\colon \begin{cases} \boldsymbol{M}\dot{\boldsymbol{u}} + \boldsymbol{C}\boldsymbol{u} = \boldsymbol{G} + \boldsymbol{F} + \boldsymbol{\Delta} \\ \dot{\boldsymbol{x}}_p = \boldsymbol{v}_p \\ \dot{\boldsymbol{R}}_{IP} = \boldsymbol{R}_{IP}\boldsymbol{\omega}_p^\times \\ \dot{\boldsymbol{r}}_j = \boldsymbol{v}_j \end{cases}; \quad \Sigma_j\colon \begin{cases} \boldsymbol{J}\dot{\boldsymbol{\omega}}_j + \boldsymbol{\omega}_j^\times\boldsymbol{J}\boldsymbol{\omega}_j = \boldsymbol{\tau}_j \\ \dot{\boldsymbol{R}}_{Ij} = \boldsymbol{R}_{Ij}\boldsymbol{\omega}_j^\times \\ \boldsymbol{f}_{L,j} = -f_j\boldsymbol{R}_{Ij}\boldsymbol{e}_3 \end{cases} \tag{2}$$

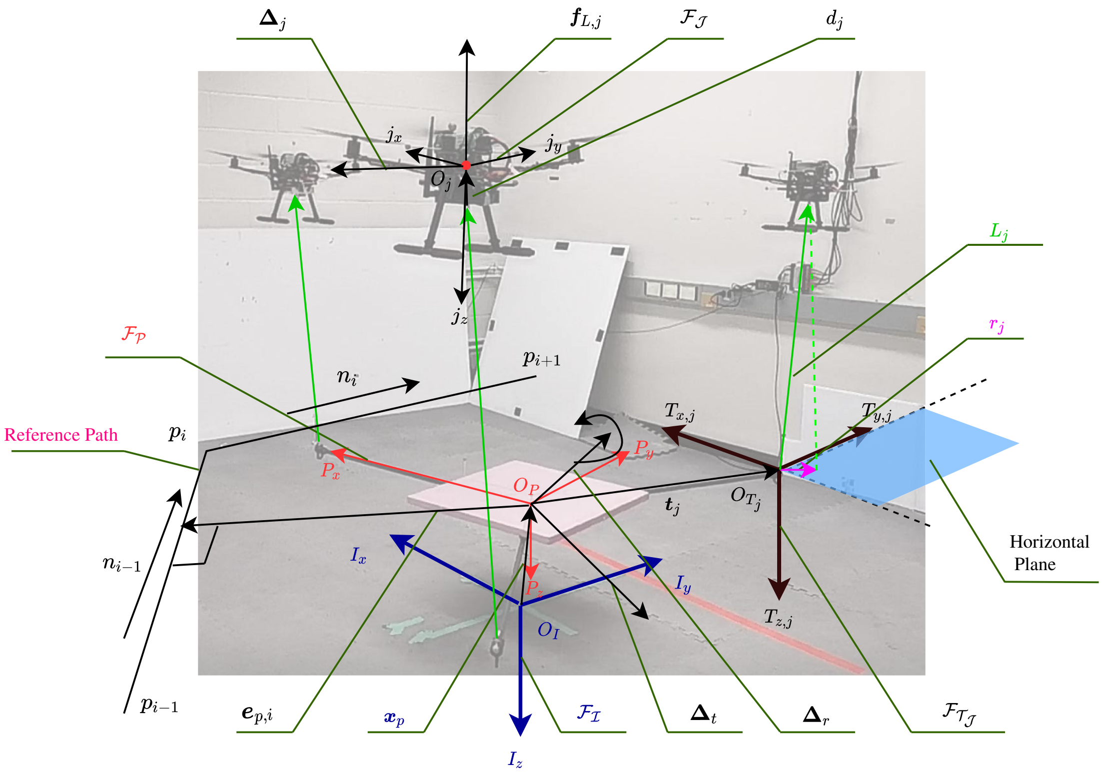

Fig. 1 The system geometry for multiple quadrotor UAVs to cooperatively carry a tethered payload. For the control design purpose, we assume $d_j \approx 0$ so that cables are attached at the CM of each quadrotor.

where the generalized speed of Σ_p is denoted by $\boldsymbol{u}$:

$$\boldsymbol{u} = \begin{bmatrix} \boldsymbol{v}_p^T & \boldsymbol{\omega}_p^T & \boldsymbol{v}_1^T & \dots & \boldsymbol{v}_N^T \end{bmatrix}^T \in \mathbb{R}^{(6+2N)\times 1} \tag{3}$$

Matrices $\boldsymbol{M}$ and $\boldsymbol{C}$ are

$$\boldsymbol{M} = \begin{bmatrix} (m_p + M_q)\mathbf{1} & \boldsymbol{R}_{IP}\boldsymbol{A}^T & m_1\boldsymbol{B}_1 & & m_N\boldsymbol{B}_N \\ \boldsymbol{A}\boldsymbol{R}_{PI} & \boldsymbol{J}_p + \boldsymbol{J}_q & m_1\boldsymbol{t}_1^\times\boldsymbol{R}_{PI}\boldsymbol{B}_1 & & m_N\boldsymbol{t}_N^\times\boldsymbol{R}_{PI}\boldsymbol{B}_N \\ m_1\boldsymbol{B}_1^T & -m_1\boldsymbol{B}_1^T\boldsymbol{R}_{IP}\boldsymbol{t}_1^\times & m_1\boldsymbol{B}_1^T\boldsymbol{B}_1 & \mathbf{0} & \mathbf{0}_{2\times 2} \\ \vdots & \vdots & \mathbf{0} & \ddots & \mathbf{0} \\ m_N\boldsymbol{B}_N^T & -m_{NN}^T\boldsymbol{R}_{IP}\boldsymbol{t}_N^\times & \mathbf{0}_{2\times 2} & \mathbf{0} & m_N\boldsymbol{B}_N^T\boldsymbol{B}_N \end{bmatrix} \in \mathbb{R}^{(6+2N)\times(6+2N)} \tag{4}$$

where $M_q = \sum_{j=1}^N m_j$, $\boldsymbol{A} = \sum_{j=1}^N m_j \boldsymbol{t}_j^\times$, and $\boldsymbol{J}_q = \sum_{j=1}^N -m_j \boldsymbol{t}_j^\times \boldsymbol{t}_j^\times$. The Coriolis effect matrix is denoted as

Finally, the generalized forces $\boldsymbol{G} \in \mathbb{R}^{(6+2N)\times 1}$, $\boldsymbol{F} \in \mathbb{R}^{(6+2N)\times 1}$, and $\boldsymbol{\Delta} \in \mathbb{R}^{(6+2N)\times 1}$ are

$$\boldsymbol{\Delta} = \begin{bmatrix} \boldsymbol{\Delta}_t + \sum_{j=1}^N \boldsymbol{\Delta}_j \\ \boldsymbol{\Delta}_r + \sum_{j=1}^N \boldsymbol{t}_j^\times \boldsymbol{R}_{PI}\boldsymbol{\Delta}_j \\ \boldsymbol{B}_1^T\boldsymbol{\Delta}_1 \\ \vdots \\ \boldsymbol{B}_N^T\boldsymbol{\Delta}_N \end{bmatrix}; \quad \boldsymbol{G} = \begin{bmatrix} m_p\boldsymbol{g}_I + \sum_{j=1}^N m_j\boldsymbol{g}_I \\ \sum_{j=1}^N m_j \boldsymbol{t}_j^\times \boldsymbol{R}_{PI}\boldsymbol{g}_I \\ m_1\boldsymbol{B}_1^T\boldsymbol{g}_I \\ \vdots \\ m_N\boldsymbol{B}_N^T\boldsymbol{g}_I \end{bmatrix};$$

$$\boldsymbol{F} = \begin{bmatrix} \sum_{j=1}^N \boldsymbol{f}_{L,j} \\ \sum_{j=1}^N \boldsymbol{t}_j^\times \boldsymbol{R}_{PI}\boldsymbol{f}_{L,j} \\ \boldsymbol{B}_1^T\boldsymbol{f}_{L,1} \\ \vdots \\ \boldsymbol{B}_N^T\boldsymbol{f}_{L,N} \end{bmatrix} \tag{6}$$

$$\boldsymbol{C} = \begin{bmatrix} \mathbf{0}_{3\times 3} & \boldsymbol{R}_{IP}\boldsymbol{\omega}_p^\times\boldsymbol{A}^T & m_1\dot{\boldsymbol{B}}_1 & \dots & m_N\dot{\boldsymbol{B}}_N \\ \mathbf{0}_{3\times 3} & -(\boldsymbol{J}_p\boldsymbol{\omega}_p)^\times - \sum_{j=1}^N m_j\boldsymbol{t}_j^\times\boldsymbol{\omega}_p^\times\boldsymbol{t}_j^\times & m_1\boldsymbol{t}_1^\times\boldsymbol{R}_{PI}\dot{\boldsymbol{B}}_1 & \dots & m_N\boldsymbol{t}_1^\times\boldsymbol{R}_{PI}\dot{\boldsymbol{B}}_N \\ \mathbf{0}_{2\times 3} & -m_1\boldsymbol{B}_1^T\boldsymbol{R}_{IP}\boldsymbol{\omega}_p^\times\boldsymbol{t}_1^\times & m_1\boldsymbol{B}_1^T\dot{\boldsymbol{B}}_1 & \mathbf{0} & \mathbf{0}_{2\times 2} \\ \vdots & \vdots & \mathbf{0} & \ddots & \mathbf{0} \\ \mathbf{0}_{2\times 3} & -m_N\boldsymbol{B}_N^T\boldsymbol{R}_{IP}\boldsymbol{\omega}_p^\times\boldsymbol{t}_N^\times & \mathbf{0}_{2\times 2} & \mathbf{0} & m_N\boldsymbol{B}_N^T\dot{\boldsymbol{B}}_N \end{bmatrix} \in \mathbb{R}^{(6+2N)\times(6+2N)} \tag{5}$$

Assumption 1: All disturbances are bounded. $\boldsymbol{\Delta}_{\perp,j}$ and $\boldsymbol{\Delta}_{\parallel,j}$ are the components of $\boldsymbol{\Delta}_j$ that are perpendicular and parallel to $\boldsymbol{L}_j$, respectively. The so-called effective disturbances on the payload are denoted as $\boldsymbol{\Delta}_T$ and $\boldsymbol{\Delta}_R$. They are calculated as follows:

$$\begin{cases}\boldsymbol{\Delta}_{\parallel,j}=\boldsymbol{L}_j\boldsymbol{L}_j^T\boldsymbol{\Delta}_j/l^2\\ \boldsymbol{\Delta}_{\perp,j}=\boldsymbol{\Delta}_j-\boldsymbol{\Delta}_{\parallel,j}\end{cases};\qquad \begin{cases}\boldsymbol{\Delta}_T=\boldsymbol{\Delta}_t+\sum_{j=1}^N\boldsymbol{\Delta}_{\parallel,j}\\ \boldsymbol{\Delta}_R=\boldsymbol{\Delta}_r+\sum_{j=1}^N\boldsymbol{t}_j^\times\boldsymbol{R}_{PI}\boldsymbol{\Delta}_{\parallel,j}\end{cases} \tag{7}$$

$\boldsymbol{\Delta}_T$ and $\boldsymbol{\Delta}_R$ can be viewed as force and torque solely acting on the payload. $\dot{\boldsymbol{\Delta}}_T\approx\mathbf{0}$, $\dot{\boldsymbol{\Delta}}_R\approx\mathbf{0}$, and $\dot{\boldsymbol{\Delta}}_j\approx\mathbf{0}$ are assumed as reasonable engineering treatments near hover in near-calm winds for a typical ADRC design [29]. The following identities are used in the subsequent stability analysis:

$$\begin{aligned}&\boldsymbol{\Delta}_t+\sum_{j=1}^N\boldsymbol{\Delta}_j=\boldsymbol{\Delta}_T+\sum_{j=1}^N\boldsymbol{\Delta}_{\perp,j};\\ &\boldsymbol{\Delta}_r+\sum_{j=1}^N\boldsymbol{t}_j^\times\boldsymbol{R}_{PI}\boldsymbol{\Delta}_j=\boldsymbol{\Delta}_R+\sum_{j=1}^N\boldsymbol{t}_j^\times\boldsymbol{R}_{PI}\boldsymbol{\Delta}_{\perp,j}\end{aligned} \tag{8}$$

D. Formulation of the Path-Following Problem

The PFP task requires the CM of the payload to travel along a path $\mathbb{P}=\{\boldsymbol{n}_i,\boldsymbol{v}_{d,i},\boldsymbol{p}_i\}(i=1,\dots,N_p)$ described by a series of interconnecting straight lines determined by the directional vectors $\boldsymbol{n}_i$ and starting waypoints $\boldsymbol{p}_i$ as shown in Fig. 1. The equilibrium of the system is the state where the payload cruises on the given reference path instead of chasing a moving reference point. $\boldsymbol{e}_{p,i}$ and $\boldsymbol{e}_{v,i}$ are defined as

$$\begin{aligned}&\boldsymbol{e}_{p,i}=\left(\boldsymbol{x}_p-\boldsymbol{p}_i-[\boldsymbol{n}_i^T(\boldsymbol{x}_p-\boldsymbol{p}_i)]\cdot\boldsymbol{n}_i\right)=(\mathbf{1}-\boldsymbol{n}_i\boldsymbol{n}_i^T)(\boldsymbol{x}_p-\boldsymbol{p}_i);\\ &\boldsymbol{e}_{v,i}=\boldsymbol{v}_p-\boldsymbol{v}_{d,i}\end{aligned} \tag{9}$$

The matrix $\mathbf{1}-\boldsymbol{n}_i\boldsymbol{n}_i^T$ extracts the component of a vector that is perpendicular to the reference line. Eliminating $\boldsymbol{e}_{p,i}$ means that the payload will slide on the path. The sliding speed of the payload is constrained by $\boldsymbol{e}_{v,i}$. The desired attitude of the slung load is denoted as a target rotation matrix $\boldsymbol{R}_{IP,d}\in SO(3)$. The attitude error $\boldsymbol{e}_r\in\mathbb{R}^{3\times1}$ becomes

$$\boldsymbol{e}_r=(\boldsymbol{R}_{PI,d}\boldsymbol{R}_{IP}-\boldsymbol{R}_{PI}\boldsymbol{R}_{IP,d})^\vee/2 \tag{10}$$

If the slung load is pushed by a horizontal disturbance force, there is a nonzero cable inclination angle at the equilibrium point for each cable. This angle is denoted as a target horizontal cable tip displacement $\boldsymbol{r}_{j,d}$, and $\boldsymbol{r}_j$ should reach $\boldsymbol{r}_{j,d}$ at the equilibrium. The cable tip movement error is defined as $\tilde{\boldsymbol{r}}_j=\boldsymbol{r}_j-\boldsymbol{r}_{j,d}$. The error state of the system is $\tilde{\boldsymbol{\mathcal{X}}}_p=\{\boldsymbol{e}_{p,i},\boldsymbol{e}_r,\tilde{\boldsymbol{r}}_1,\dots,\tilde{\boldsymbol{r}}_N,\boldsymbol{e}_{v,i},\boldsymbol{\omega}_p,\boldsymbol{v}_1,\dots,\boldsymbol{v}_N\}$. The PFP is then defined as follows: for given a path $\mathbb{P}$, design $\boldsymbol{f}_{L,j}$ such that the equilibrium $\tilde{\boldsymbol{\mathcal{X}}}_p^\star=\{\mathbf{0},\mathbf{0},\mathbf{0},\mathbf{0},\dots,\mathbf{0}\}$ is asymptotically stable (AS).

III. Controller Design

This section presents the controller design. The proposed control law has a hierarchical structure. A virtual control force is first provided based on the payload path and attitude error. Once the virtual control law provides the reference lift vector, the attitude controller of each quadrotor tilts the quadrotor accordingly to control the payload.

A. Configuration Requirement

To fully control the load attitude, at least three quadrotors are needed. The condition for fully payload controllability is that there exist scalars $a_j>0$ and an auxiliary matrix $\boldsymbol{D}$ such that

$$\sum_{j=1}^N a_j\boldsymbol{t}_j=\mathbf{0};\qquad \sum_{j=1}^N a_j=1;\qquad \boldsymbol{D}=\sum_{j=1}^N a_j\boldsymbol{t}_j^\times\boldsymbol{t}_j^\times;\qquad \mathrm{rank}(\boldsymbol{D})=3 \tag{11}$$

The above condition ensures that the cables are distributed around the CM of the payload so that the payload can be leveled during flight. This property is similar to the rank condition in Eq. (13) of Ref. [13] but can be directly used in controller design. Consequently, $\forall\boldsymbol{b}\in\mathbb{R}^{3\times1}$, and the following is true:

$$\sum_{j=1}^N a_j\boldsymbol{t}_j^\times\boldsymbol{b}=-\boldsymbol{b}^\times\sum_{j=1}^N a_j\boldsymbol{t}_j=\mathbf{0};\quad \sum_{j=1}^N a_j\boldsymbol{b}=\boldsymbol{b} \tag{12}$$

This property is later used in Eqs. (15) and (18) to distribute the lifting force to cancel gravity without introducing net moment on the payload. A constant matrix $\boldsymbol{E}_j$, which is used subsequently in control design, is defined as

$$\boldsymbol{E}_j=\boldsymbol{t}_j^\times\boldsymbol{D}^{-1};\ \sum_{j=1}^N a_j\boldsymbol{E}_j=\mathbf{0};\ \sum_{j=1}^N a_j\boldsymbol{t}_j^\times\boldsymbol{E}_j=\left[\sum_{j=1}^N a_j\boldsymbol{t}_j^\times\boldsymbol{t}_j^\times\right]\boldsymbol{D}^{-1}=\mathbf{1} \tag{13}$$

Similar to the property in Eq. (12), $\boldsymbol{E}_j$ is used in Eqs. (15) and (18) to distribute the control torque to each drone without adding residue force.

B. Virtual Control Force

First, the virtual control law needs the following auxiliary variables: k_L, k_v, and k_r are positive gains. The "^" symbol is used to annotate terms with the estimated disturbances.

$$\begin{cases}\boldsymbol{s}_p=\boldsymbol{e}_{v,i}+k_v\boldsymbol{e}_{p,i}\\ \boldsymbol{s}_r=\boldsymbol{\omega}_p+k_r\boldsymbol{e}_r\\ \hat{\boldsymbol{\mu}}_j=k_L(\boldsymbol{r}_j-\hat{\boldsymbol{r}}_{j,d})\end{cases};\quad \begin{cases}\hat{\boldsymbol{R}}_1=\sum_{j=1}^N a_j\boldsymbol{B}_j(\boldsymbol{v}_j+\hat{\boldsymbol{\mu}}_j)\\ \dot{\hat{\boldsymbol{F}}}_1=-\lambda_1\hat{\boldsymbol{F}}_1+k_{r1}\hat{\boldsymbol{R}}_1\\ \dot{\hat{\boldsymbol{\xi}}}=k_v\dot{\boldsymbol{e}}_{p_i}+\dot{\hat{\boldsymbol{F}}}_1\\ \hat{\boldsymbol{\xi}}=k_v\boldsymbol{e}_{p_i}+\hat{\boldsymbol{F}}_1-\boldsymbol{v}_{d,i}\end{cases};$$

$$\begin{cases}\hat{\boldsymbol{R}}_2=\sum_{j=1}^N a_j\boldsymbol{E}_j^T\boldsymbol{R}_{PI}\boldsymbol{B}_j(\boldsymbol{v}_j+\hat{\boldsymbol{\mu}}_j)\\ \dot{\hat{\boldsymbol{F}}}_2=-\lambda_2\hat{\boldsymbol{F}}_2+k_{r2}\hat{\boldsymbol{R}}_2\\ \dot{\hat{\boldsymbol{\eta}}}=k_r\dot{\boldsymbol{e}}_r+\dot{\hat{\boldsymbol{F}}}_2\\ \hat{\boldsymbol{\eta}}=k_r\boldsymbol{e}_r+\hat{\boldsymbol{F}}_2\end{cases} \tag{14}$$

$\lambda_1,\lambda_2,K_0,k_p$, and k_Ω are positive numbers; $\boldsymbol{s}_p,\boldsymbol{s}_r$, and $\hat{\boldsymbol{\mu}}_j$ are the path-following error, the attitude error, and the quadrotor position error relative to the payload. Then the virtual control law $\boldsymbol{f}_{v,j}$ becomes

$$\begin{cases}\boldsymbol{f}_{v,j}=\hat{\boldsymbol{f}}_{0,j}+\boldsymbol{f}_{a,j}+\boldsymbol{f}_{b,j}+\boldsymbol{f}_{c,j}+\hat{\boldsymbol{f}}_{t,j}\\ \hat{\boldsymbol{f}}_{0,j}=-m_j\left[\dot{\hat{\boldsymbol{\xi}}}+k_L\boldsymbol{B}_j\boldsymbol{v}_j+\dot{\boldsymbol{B}}_j\hat{\boldsymbol{\mu}}_j-d(\boldsymbol{R}_{IP}\boldsymbol{t}_j^\times\hat{\boldsymbol{\eta}})/dt\right]\\ \boldsymbol{f}_{a,j}=-K_0\left[\boldsymbol{v}_p+\hat{\boldsymbol{\xi}}-\boldsymbol{R}_{IP}\boldsymbol{t}_j^\times(\boldsymbol{\omega}_p+\hat{\boldsymbol{\eta}})+\boldsymbol{B}_j(\boldsymbol{v}_j+\hat{\boldsymbol{\mu}}_j)\right]\\ \boldsymbol{f}_{b,j}=-a_j\left(m_p\dot{\hat{\boldsymbol{\xi}}}+k_pm_p\boldsymbol{s}_p\right)\\ \boldsymbol{f}_{c,j}=-a_j\boldsymbol{R}_{IP}\boldsymbol{E}_j\left(\boldsymbol{J}_p\dot{\hat{\boldsymbol{\eta}}}+k_\Omega\boldsymbol{s}_r\right)\end{cases} \tag{15}$$

Here $\boldsymbol{f}_{v,j}$ consists of three parts with their physical meanings; $\hat{\boldsymbol{f}}_{t,j}$ is the trimming force that balances the total gravity and disturbance; $\hat{\boldsymbol{f}}_{0,j}$ synchronizes motion of the quadrotor to the payload; $\boldsymbol{f}_{a,j}$, $\boldsymbol{f}_{b,j}$, and $\boldsymbol{f}_{c,j}$ eliminate the path error of the payload. As the filtered results of $\hat{\boldsymbol{R}}_1$ and $\hat{\boldsymbol{R}}_2$, $\hat{\boldsymbol{\zeta}}$, and $\hat{\boldsymbol{\eta}}$ are the motion cross-feeding terms to correct the control lift according to the cable inclination angles. If cables incline to a direction such that the tension forces are reducing the path error, $\hat{\boldsymbol{R}}_1$ and $\hat{\boldsymbol{R}}_2$ will reduce the total control force, and vice versa. The actual torque and lift that the propeller should generate is given in Sec. III.E. The expressions of $\hat{\boldsymbol{r}}_{j,d}$ and $\hat{\boldsymbol{f}}_{t,j}$ are presented in the following sections.

C. Disturbance Estimation Law

This section provides the update laws for the disturbance estimator based on the UDE technique [6]. The estimated disturbances are defined as $\hat{\boldsymbol{\Delta}}_T$, $\hat{\boldsymbol{\Delta}}_R$, and $\hat{\boldsymbol{\Delta}}_{\perp,j}$. Let $\mathfrak{B}_j = \boldsymbol{B}_j(\boldsymbol{B}_j^T\boldsymbol{B}_j)^{-1}\boldsymbol{B}_j^T$ be a series of auxiliary matrices. The update law of $\hat{\boldsymbol{\Delta}}_{\perp,j}$ is

$$\hat{\boldsymbol{\Delta}}_{\perp,j} = (\boldsymbol{1} - \boldsymbol{L}_j\boldsymbol{L}_j^T/l^2)\hat{\boldsymbol{\Delta}}_j;$$
$$\hat{\boldsymbol{\Delta}}_j = \int_0^t \kappa_j \mathfrak{B}_j\left(m_j\dot{\boldsymbol{v}}_{q,j} - \boldsymbol{f}_{L,j} - m_j\boldsymbol{g}_I - \hat{\boldsymbol{\Delta}}_j\right)\mathrm{d}\tau \tag{16}$$

where $\dot{\boldsymbol{v}}_{q,j}$ is the acceleration of each quadrotor measured by the on-board IMU expressed in $\mathcal{F}_{\mathcal{I}}$. It can be calculated using the attitude of the quadrotor and the raw acceleration feedback; κ_j is a positive rate constant. Here $\boldsymbol{f}_{L,j}$ is the actual lift calculated based on the thrust model from system identification and quadrotor attitude. The expressions of $\hat{\boldsymbol{\Delta}}_T$ and $\hat{\boldsymbol{\Delta}}_R$ become

$$\begin{aligned}
\hat{\boldsymbol{\Delta}}_T = \lambda_T\Bigg[&(m_p + M_q)\boldsymbol{v}_p + \boldsymbol{R}_{IP}\boldsymbol{A}^T\boldsymbol{\omega}_p + \sum_{j=1}^N m_j\boldsymbol{B}_j\boldsymbol{v}_j \\
&- \int_0^t \sum_{j=1}^N\left(\boldsymbol{f}_{L,j} + \hat{\boldsymbol{\Delta}}_{\perp,j}\right) + \hat{\boldsymbol{\Delta}}_T + (m_p + M_q)\boldsymbol{g}_I\,\mathrm{d}\tau\Bigg]; \\
\hat{\boldsymbol{\Delta}}_R = \lambda_R\Bigg[&\int_0^t \boldsymbol{A}\boldsymbol{\omega}_p^\times\boldsymbol{R}_{PI}\boldsymbol{v}_p + \boldsymbol{\omega}_p^\times\boldsymbol{J}_p\boldsymbol{\omega}_p - \hat{\boldsymbol{\Delta}}_R \\
&+ \sum_{j=1}^N \boldsymbol{t}_j^\times\Big(m_j\left(\boldsymbol{\omega}_p^\times\boldsymbol{R}_{PI}\boldsymbol{B}_j\boldsymbol{v}_j - \boldsymbol{\omega}_p^\times\boldsymbol{t}_j^\times\boldsymbol{\omega}_p - \boldsymbol{R}_{PI}\boldsymbol{g}_I\right) \\
&- \boldsymbol{R}_{PI}\left(\boldsymbol{f}_{L,j} + \hat{\boldsymbol{\Delta}}_{\perp,j}\right)\Big)\mathrm{d}\tau + \boldsymbol{A}\boldsymbol{R}_{PI}\boldsymbol{v}_p + (\boldsymbol{J}_q + \boldsymbol{J}_p)\boldsymbol{\omega}_p \\
&+ \sum_{j=1}^N m_j\boldsymbol{t}_j^\times\boldsymbol{R}_{PI}\boldsymbol{B}_j\boldsymbol{v}_j\Bigg]
\end{aligned} \tag{17}$$

where λ_T and λ_R are positive rate constants defined in the subsequent stability analysis section. The update laws are straightforward solutions of Eqs. (42), (43), and (36). Intuitively, the integral terms of the disturbance estimator accumulate the path-following error of the payload and can be viewed as a nonlinear PID controller with guaranteed stability.

D. Equilibrium Lift Forces

At the equilibrium, $\boldsymbol{G} + \boldsymbol{F} + \boldsymbol{\Delta} = \boldsymbol{0}$. According to Eq. (7), $\boldsymbol{B}_j^T\boldsymbol{\Delta}_{\|,j} = 0$, so $\boldsymbol{\Delta}_{\|,j}$ does not affected the cable rotation; $\hat{\boldsymbol{f}}_{d,j}$ balances the estimated disturbances and weight of the payload; $\hat{\boldsymbol{f}}_{t,j}$ is the total lift of each quadrotor at the equilibrium. The equilibrium point of $\boldsymbol{r}_j$ is defined as $\hat{\boldsymbol{r}}_{j,d}$.

$$\hat{\boldsymbol{f}}_{d,j} = -a_j\left(m_p\boldsymbol{g}_I + \hat{\boldsymbol{\Delta}}_T + \boldsymbol{R}_{IP}\boldsymbol{E}_j\hat{\boldsymbol{\Delta}}_R\right);\quad \hat{\boldsymbol{f}}_{t,j} = -m_j\boldsymbol{g}_I + \hat{\boldsymbol{f}}_{d,j} - \hat{\boldsymbol{\Delta}}_{\perp,j};$$
$$\hat{\boldsymbol{r}}_{j,d} = l(\hat{\boldsymbol{f}}_{d,j})_{xy}/\|\hat{\boldsymbol{f}}_{d,j}\| \tag{18}$$

Here $\hat{\boldsymbol{f}}_{t,j}$ is picked so that all cables are vertical if the disturbances are zero, providing the best thrust efficiency.

E. Quadrotor Attitude Control Law

This section presents the target torque and lift each quadrotor should generate as shown in Fig. 2. The total lift from the propellers is $f_j = \|\boldsymbol{f}_{v,j}\|$. A command yaw angle ψ is picked for each quadrotor. The lift is assumed along the $-z$ axis of the quadrotor, i.e., $\boldsymbol{n}_z = -\boldsymbol{f}_{v,j}/f_j$. The reference attitude trajectory of each quadrotor based on $\boldsymbol{f}_{v,j}$ is $\boldsymbol{R}_{Ij,d}$, obtained in the following way:

$$\tilde{\boldsymbol{n}}_x = \begin{bmatrix}\cos\psi & \sin\psi & -(\cos\psi n_{z,x} + \sin\psi n_{z,y})/n_{z,z}\end{bmatrix}^T;$$
$$\boldsymbol{n}_x = \tilde{\boldsymbol{n}}_x/\|\tilde{\boldsymbol{n}}_x\|;\quad \boldsymbol{n}_y = \boldsymbol{n}_z^\times\boldsymbol{n}_x/\|\boldsymbol{n}_z^\times\boldsymbol{n}_x\|;\quad \boldsymbol{R}_{Ij,d} = [\boldsymbol{n}_x \quad \boldsymbol{n}_y \quad \boldsymbol{n}_z] \tag{19}$$

where $\boldsymbol{n}_{z,x}$ and $\boldsymbol{n}_{z,y}$ are the x and y components of $\boldsymbol{n}_z$, respectively; $\boldsymbol{f}_{v,j}$ only provides two degrees of freedom (i.e., $\boldsymbol{n}_z$), so ψ is an additional constraint to determine $\boldsymbol{R}_{Ij,d}$. We define $\boldsymbol{\omega}_{d,j}$ as the desired angular velocity, and $\tilde{\mathcal{X}}_{\mathrm{rot},j} = \{\tilde{\boldsymbol{\omega}}_j, \boldsymbol{R}_j\}$ as the error state of Σ_j. Once $\boldsymbol{R}_{Ij,d}$, $\boldsymbol{\omega}_{d,j}$, and $\dot{\boldsymbol{\omega}}_{d,j}$ are calculated based on $\boldsymbol{f}_{v,j}$, an almost global asymptotically stable (AGAS) attitude tracker as suggested in Sec. VI.C of Ref. [30] is used:

$$\boldsymbol{\tau}_j = -b_\omega\tilde{\boldsymbol{\omega}}_j - b_r\boldsymbol{e}_{r,j} - \tilde{\boldsymbol{\omega}}_j^\times\boldsymbol{J}\tilde{\boldsymbol{\omega}}_j + \boldsymbol{\omega}_j^\times\boldsymbol{J}\boldsymbol{\omega}_j - \boldsymbol{J}\left(\tilde{\boldsymbol{\omega}}_j^\times\tilde{\boldsymbol{R}}_j^T\boldsymbol{\omega}_{d,j} - \tilde{\boldsymbol{R}}_j^T\dot{\boldsymbol{\omega}}_{d,j}\right) \tag{20}$$

where $\boldsymbol{e}_{r,j} = \sum_{i=1}^3 \boldsymbol{e}_i^\times\tilde{\boldsymbol{R}}_j\boldsymbol{e}_i$, $\tilde{\boldsymbol{R}}_j = \boldsymbol{R}_{Ij,d}^T\boldsymbol{R}_{Ij}$, $\boldsymbol{\omega}_{d,j} = (\boldsymbol{R}_{Ij,d}^T\dot{\boldsymbol{R}}_{Ij,d})^\vee$, and $\tilde{\boldsymbol{\omega}}_j = \boldsymbol{\omega}_j - \boldsymbol{R}_j^T\boldsymbol{\omega}_{d,j}$; b_ω and b_r are positive control gains. The attitude tracker design in Eq. (20) is decoupled from the design of $\boldsymbol{f}_{v,j}$, providing the freedom to implement a variety of robust attitude trackers without redoing the stability analysis.

IV. Stability Analysis

This section provides the stability analysis for the closed-loop system. First, a Lyapunov function candidate is provided with each term representing the equilibrium of the system. Then time derivatives of the Lyapunov function are derived and shown to be negative semidefinite. Finally, the attitude tracking law is added and the stability of the complete system is shown using the reduction theorem.

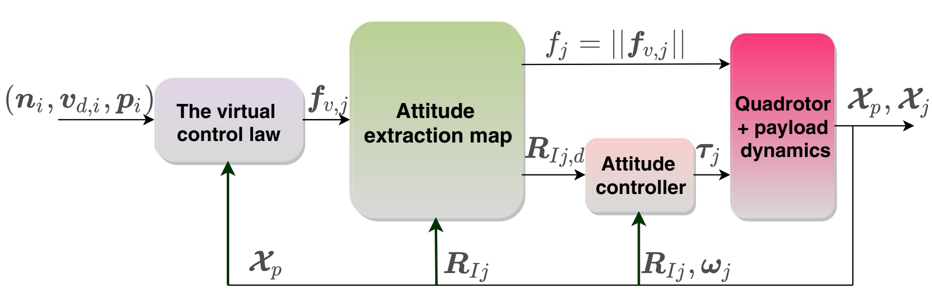

Fig. 2 The control diagram for the system.

A. Lyapunov Function Candidate

Remark 1: It is crucial to clarify that the closed-loop system is locally asymptotically stable when disturbances are bounded. An angle $\theta_{\max} = \arccos(1/\delta_r)$, where $\delta_r > 1$ is defined as the range of the cable tip motion, i.e., $\|\boldsymbol{r}_j\|/l \le \sqrt{1 - 1/\delta_r^2}$. The limit of cable swing velocity is $\|\boldsymbol{v}_j\|/l \le \delta_v$, and the range of payload angular velocity is $\|\boldsymbol{\omega}_p\| \le \delta_\omega$. External disturbances are assumed bounded, so θ_d is used to denote the range of $\|\boldsymbol{r}_{d,j}\|$, i.e., $\|\boldsymbol{r}_{d,j}\| = l\sin\theta_d \le l\sin\theta_{\max}$.

The following intermediate variables are used in the stability analysis:

$$\begin{cases} C_r = \tan[(\theta_{\max} + \theta_d)/2] \\ \gamma_j = \sqrt{1 + C_r^2} \\ \sigma_j = \|\boldsymbol{E}_j \boldsymbol{J}_p^{1/2}\| \end{cases}; \quad \begin{cases} \Xi_1 = \lambda_1 + k_{r1}k_{F1} \\ \Xi_2 = \lambda_2 + k_{r2}k_{F2} \\ \Gamma_c = \max_{j=1,\ldots,N}\{\|\boldsymbol{t}_j^\times\|\} \end{cases}; \quad \begin{cases} E_0 = \max_{j=1,\ldots,N}\{\|\boldsymbol{E}_j\|\} \\ G_{r,j} = \|\boldsymbol{f}_{d,j}\|(\cos\theta_d - C_r \sin\theta_d)/(la_j) \\ \delta_R = \sup(a_j \boldsymbol{E}_j \boldsymbol{\Delta}_R / \|\boldsymbol{f}_{d,j}\|) \end{cases} \tag{21}$$

Lemma 1: The following properties are true (a proof can be found in the Appendix of Ref. [31]):

i) $(\boldsymbol{L}_{j,d} - \boldsymbol{L}_j)^T(\boldsymbol{L}_{j,d} - \boldsymbol{L}_j)/(2l) = (l - \boldsymbol{L}_{j,d}^T\boldsymbol{L}_j/l)$.

ii) $\|\boldsymbol{B}_j\boldsymbol{x}\| \le \delta_r\|\boldsymbol{x}\|$ and $\|\dot{\boldsymbol{B}}_j\boldsymbol{x}\| \le \delta_r^3\delta_v\|\boldsymbol{x}\|, \forall\, \boldsymbol{x} \in \mathbb{R}^{2\times 1}$.

iii) If $C_r = \tan[(\theta_{\max} + \theta_d)/2]$, then $C_r\|\tilde{\boldsymbol{r}}_j\| \ge |\sqrt{l^2 - \boldsymbol{r}_j^2} - \sqrt{l^2 - \boldsymbol{r}_{j,d}^2}|$ and $\|\boldsymbol{L}_{j,d} - \boldsymbol{L}_j\| \le \sqrt{1 + C_r^2}\|\tilde{\boldsymbol{r}}_j\| = \gamma_j\|\tilde{\boldsymbol{r}}_j\|$.

iv) $\forall \boldsymbol{x} \in \mathbb{R}^{3\times 1} \ne 0$, we define $\boldsymbol{x}_\perp$ and $\boldsymbol{x}_\parallel$ as its components perpendicular and parallel to $\boldsymbol{L}_j$. Then $\boldsymbol{x}^T\mathfrak{B}_j\boldsymbol{x} = \boldsymbol{x}_\perp^T\boldsymbol{x}_\perp$.

v) $\|\dot{\boldsymbol{e}}_{p,i}\| \le \|\boldsymbol{e}_{v,i}\|$, $\|\dot{\boldsymbol{e}}_r\| \le \|\boldsymbol{\omega}_p\|$.

Several additional auxiliary variables are defined as counter parts of the variables in Eq. (14). These auxiliary variables use the true disturbances forces and are only used in the stability analysis:

$$\begin{cases} \boldsymbol{R}_1 = \sum_{j=1}^N a_j\boldsymbol{B}_j(\boldsymbol{v}_j + \boldsymbol{\mu}_j) \\ \dot{\boldsymbol{F}}_1 = -\lambda_1\boldsymbol{F}_1 + k\boldsymbol{R}_1 \\ \dot{\boldsymbol{\zeta}} = k_v\dot{\boldsymbol{e}}_{p_i} + \dot{\boldsymbol{F}}_1 \\ \boldsymbol{\zeta} = k_v\boldsymbol{e}_{p_i} + \boldsymbol{F}_1 - \boldsymbol{v}_{d,i} \end{cases}; \quad \begin{cases} \boldsymbol{R}_2 = \sum_{j=1}^N a_j\boldsymbol{E}_j^T\boldsymbol{R}_{PI}\boldsymbol{B}_j(\boldsymbol{v}_j + \boldsymbol{\mu}_j) \\ \dot{\boldsymbol{F}}_2 = -\lambda_2\boldsymbol{F}_2 + k_{r2}\boldsymbol{R}_2 \\ \dot{\boldsymbol{\eta}} = k_r\dot{\boldsymbol{e}}_r + \dot{\boldsymbol{F}}_2 \\ \boldsymbol{\eta} = k_r\boldsymbol{e}_r + \boldsymbol{F}_2 \end{cases}; \quad \begin{cases} \boldsymbol{\mu}_j = k_L\tilde{\boldsymbol{r}}_j \\ \dot{\boldsymbol{\mu}}_j = k_L(\boldsymbol{v}_j - \dot{\boldsymbol{r}}_{j,d}) \end{cases} \tag{22}$$

The true equilibrium force $\boldsymbol{f}_{d,j}$, $\boldsymbol{r}_{j,d}$, and the estimation error of the cable equilibrium $\tilde{\boldsymbol{r}}_{j,d}$ are defined as

$$\begin{cases} \boldsymbol{f}_{0,j} = -m_j[\dot{\boldsymbol{\zeta}} + d(\boldsymbol{B}_j\boldsymbol{\mu}_j)/dt - d(\boldsymbol{R}_{IP}\boldsymbol{t}_j^\times\boldsymbol{\eta})/dt] \\ \boldsymbol{f}_{d,j} = -a_j(m_p\boldsymbol{g}_I + \boldsymbol{D}_T + \boldsymbol{R}_{IP}\boldsymbol{E}_j\boldsymbol{\Delta}_R) \end{cases}; \quad \begin{cases} \boldsymbol{r}_{j,d} = l(\boldsymbol{f}_{d,j,xy}/\|\boldsymbol{f}_{d,j}\|) \\ \tilde{\boldsymbol{r}}_{j,d} = \hat{\boldsymbol{r}}_{j,d} - \boldsymbol{r}_{j,d} \end{cases} \tag{23}$$

Then the Lyapunov function candidate is denoted as $V = V_1 + [\sum_{j=1}^N a_jV_{2,j}] + V_3 + V_4$. Its subterms V_1, $V_{2,j}$, V_3, and V_4 are as follows:

$$V_1 = \frac{1}{2}(\boldsymbol{u} + \boldsymbol{u}_d)^T\boldsymbol{M}(\boldsymbol{u} + \boldsymbol{u}_d) \tag{24}$$

where $\boldsymbol{u}_d = [\boldsymbol{\zeta}^T \quad \boldsymbol{\eta}^T \quad \boldsymbol{\mu}_1^T \quad \ldots \quad \boldsymbol{\mu}_N^T]^T$ is defined as a counterpart of $\boldsymbol{u}$ in Eq. (3). V_1 can be viewed as the penalty for the position and velocity error of the payload. The residue between the true and estimated auxiliary variables are $\tilde{\boldsymbol{F}}_1 = \hat{\boldsymbol{F}}_1 - \boldsymbol{F}_1$, $\tilde{\boldsymbol{R}}_1 = \hat{\boldsymbol{R}}_1 - \boldsymbol{R}_1$, $\tilde{\boldsymbol{F}}_2 = \hat{\boldsymbol{F}}_2 - \boldsymbol{F}_2$, and $\tilde{\boldsymbol{R}}_2 = \hat{\boldsymbol{R}}_2 - \boldsymbol{R}_2$. We also define $\tilde{\boldsymbol{L}}_j = \boldsymbol{L}_{j,d} - \boldsymbol{L}_j$, $\boldsymbol{\mathcal{F}}_2 = \boldsymbol{J}_p^{1/2}\boldsymbol{F}_2$, and $\mathcal{R}_2 = \boldsymbol{J}_p^{1/2}\boldsymbol{R}_2$. Ξ_1, Ξ_2 are defined in Eq. (21). $\boldsymbol{J}_p^{1/2}$ is the square root of $\boldsymbol{J}_p$, i.e., $\boldsymbol{J}_p^{1/2}\boldsymbol{J}_p^{1/2} = \boldsymbol{J}_p$. According to Lemma 1 (i), V_2 is then constructed and bounded as follows:

$$\begin{aligned} V_{2,j} &= m_p\Xi_1\tilde{\boldsymbol{L}}_j^T\boldsymbol{F}_1 + \frac{1}{2}m_pk_{F1}\boldsymbol{F}_1^T\boldsymbol{F}_1 + \frac{1}{2}k_{F2}\boldsymbol{F}_2^T\boldsymbol{J}_p\boldsymbol{F}_2 \\ &\quad + \Xi_2\tilde{\boldsymbol{L}}_j^T\boldsymbol{R}_{IP}\boldsymbol{E}_j\boldsymbol{J}_p\boldsymbol{F}_2 + \|\boldsymbol{f}_{d,j}\| \cdot (l - \boldsymbol{L}_{j,d}^T\boldsymbol{L}_j/l)/a_j. \\ &\ge \|\boldsymbol{f}_{d,j}\| \cdot \|\tilde{\boldsymbol{L}}_j\|^2/(4a_jl) - m_p\Xi_1\|\tilde{\boldsymbol{L}}_j\| \cdot \|\boldsymbol{F}_1\| + m_pk_{F1}\boldsymbol{F}_1^2/2 \\ &\quad + \|\boldsymbol{f}_{d,j}\| \cdot \|\tilde{\boldsymbol{L}}_j\|^2/(4a_jl) - \Xi_2\|\boldsymbol{E}_j\boldsymbol{J}_p^{1/2}\| \cdot \|\tilde{\boldsymbol{L}}_j\| \cdot \|\boldsymbol{\mathcal{F}}_2\| \\ &\quad + k_{F2}\boldsymbol{\mathcal{F}}_2^2/2 \end{aligned} \tag{25}$$

$V_{2,j}$ is positive definite if the following inequality holds:

$$\|\boldsymbol{f}_{d,j}\|/(2a_jl) > \max\left\{\Xi_1^2m_p/k_{F1}, \Xi_2^2\sigma_j^2/k_{F2}\right\} \tag{26}$$

where σ_j is defined in Eq. (21). V_2 denotes the penalty of on the difference of the desired and current cable inclination angles. V_3 is defined as the penalty on the path-following and attitude stabilization error:

$$V_3 = k_pk_vm_p\boldsymbol{e}_{p,i}^2 + k_rk_\Omega tr\left(\boldsymbol{1} - \boldsymbol{R}_{PI,d}^T\boldsymbol{R}_{PI}\right) \tag{27}$$

The errors of the disturbance estimation are defined as $\tilde{\boldsymbol{\Delta}}_T = \hat{\boldsymbol{\Delta}}_T - \boldsymbol{\Delta}_T$, $\tilde{\boldsymbol{\Delta}}_R = \hat{\boldsymbol{\Delta}}_R - \boldsymbol{\Delta}_R$, and $\tilde{\boldsymbol{\Delta}}_j = \hat{\boldsymbol{\Delta}}_j - \boldsymbol{\Delta}_j$. Γ_c is defined in Eq. (21). Finally, V_4 is constructed by using the estimation errors as follows:

$$\begin{aligned} V_4 &= \frac{1}{2}c_T\tilde{\boldsymbol{\Delta}}_T^2 + \frac{1}{2}c_R\tilde{\boldsymbol{\Delta}}_R^2 \\ &\quad + \frac{1}{2}\sum_{j=1}^N\left((a_jc_R\lambda_RN^2\Gamma_c^2 + c_T\lambda_TN)/(2\kappa_j) + c_ja_j\right)\tilde{\boldsymbol{\Delta}}_j^2 \end{aligned} \tag{28}$$

B. Derivative of the Lyapunov Function

Now we follow the standard procedure of using the Lyapunov direct method and take the time derivative of each component in the Lyapunov function.

1. Time Derivative of V_1

Proposition 1: Considering the dynamic model in Eq. (2) and the virtual control law in Eq. (15), we can obtain the time derivative of V_1 satisfies the following inequality constraint:

$$\begin{aligned} \dot{V}_1 &\le -k_\Omega\boldsymbol{s}_r^2 - k_pm_p\boldsymbol{s}_p^2 - \boldsymbol{\eta}^T\boldsymbol{\omega}_p^\times\boldsymbol{J}_p\boldsymbol{\omega}_p - m_p\boldsymbol{R}_1^T(k_v\dot{\boldsymbol{e}}_{p,i} - \lambda_1\boldsymbol{F}_1 + k_{r1}\boldsymbol{R}_1) \\ &\quad - k_pm_p(\boldsymbol{F}_1 + \boldsymbol{R}_1)^T\boldsymbol{s}_p - \boldsymbol{R}_2^T\boldsymbol{J}_p(k_r\dot{\boldsymbol{e}}_r - \lambda_2\boldsymbol{F}_2 + k_{r2}\boldsymbol{R}_2) \\ &\quad - k_\Omega(\boldsymbol{F}_2 + \boldsymbol{R}_2)^T\boldsymbol{s}_r + \sum_{j=1}^N\Big[-K_0\boldsymbol{\Phi}_j^T\boldsymbol{\Phi}_j + \boldsymbol{v}_j\boldsymbol{B}_j^T\boldsymbol{f}_{d,j} - k_La_jG_{r,j}\tilde{\boldsymbol{r}}_j^2 \\ &\quad + \|\boldsymbol{\Phi}_j\|\Big(h_{\delta,j}\Big(\|\tilde{\boldsymbol{\Delta}}_T\| + E_0\|\tilde{\boldsymbol{\Delta}}_R\|\Big) + m_jk_L\delta_r\|\dot{\boldsymbol{r}}_{j,d}\| \\ &\quad + a_j\|\tilde{\boldsymbol{\Delta}}_T\| + a_jE_0\|\tilde{\boldsymbol{\Delta}}_R\| + \|\tilde{\boldsymbol{\Delta}}_{\perp,j}\|\Big)\Big] \end{aligned} \tag{29}$$

where $\boldsymbol{\Phi}_j$, $\hat{\boldsymbol{\Phi}}_j$, and $\tilde{\boldsymbol{\Phi}}_j$ are defined as follows:

$$\begin{aligned} \boldsymbol{\Phi}_j &= \boldsymbol{v}_p + \boldsymbol{\zeta} - \boldsymbol{R}_{IP}\boldsymbol{t}_j^\times(\boldsymbol{\omega}_p + \boldsymbol{\eta}) + \boldsymbol{B}_j(\boldsymbol{v}_j + \boldsymbol{\mu}_j); \\ \tilde{\boldsymbol{\Phi}}_j &= \hat{\boldsymbol{\Phi}}_j - \boldsymbol{\Phi}_j = \tilde{\boldsymbol{\zeta}} - \boldsymbol{R}_{IP}\boldsymbol{t}_j^\times\tilde{\boldsymbol{\eta}} + \boldsymbol{B}_j\tilde{\boldsymbol{\mu}} \end{aligned} \tag{30}$$

Proof: See Appendix A.

2. Time Derivative of $V_{2,j}$

Proposition 2: Considering the dynamic model in Eq. (2), the virtual control law in Eq. (15), and the definition of the auxiliary variables in Eq. (22), we can obtain an upper bound of $\dot{V}_2$ as

$$\begin{aligned}\sum_{j=1}^{N} a_j \dot{V}_{2,j} \le & -m_p k_{F1}\lambda_1 \boldsymbol{F}_1^2 - \lambda_2 k_{F2}\boldsymbol{\mathcal{F}}_2^2 - \lambda_1 m_p \boldsymbol{R}_1^T \boldsymbol{F}_1 - \lambda_2 \boldsymbol{R}_2^T \boldsymbol{J}_p \boldsymbol{F}_2 \\ & - \sum_{j=1}^{N} \boldsymbol{f}_{d,j}^T \boldsymbol{B}_j v_j + \sum_{j=1}^{N} a_j \Big[\gamma_j \|\boldsymbol{E}_j \boldsymbol{\Delta}_R\| \cdot \|\boldsymbol{\omega}_p\| \cdot \|\tilde{\boldsymbol{r}}_j\| \\ & + \Xi_1 \gamma_j m_p k_{r1} \|\tilde{\boldsymbol{r}}_j\| \cdot \|\boldsymbol{R}_1\| + \Xi_1 m_p (\delta_r k_L + \lambda_1 \gamma_j) \|\tilde{\boldsymbol{r}}_j\| \cdot \|\boldsymbol{F}_1\| \\ & + m_p \Xi_1 l \|\boldsymbol{\omega}_p\| \cdot \|\boldsymbol{F}_1\| \delta_R + \Xi_2 \gamma_j \sigma_j k_{r2} \|\tilde{r}_j\| \cdot \|\mathcal{R}_2\| \\ & + \Xi_2 \sigma_j (\delta_r k_L + \gamma_j \delta_\omega + \lambda_2 \gamma_j) \|\tilde{\boldsymbol{r}}_j\| \cdot \|\boldsymbol{\mathcal{F}}_2\| \\ & + \Xi_2 \sigma_j \delta_R l \|\boldsymbol{\omega}_p\| \cdot \|\boldsymbol{\mathcal{F}}_2\| \Big] \end{aligned} \tag{31}$$

Proof: See Appendix B.

3. Time Derivative of V_3

$$\dot{V}_3 = 2k_p k_v m_p \boldsymbol{e}_{p_i}^T \dot{\boldsymbol{e}}_{p_i} + 2k_r k_\Omega \boldsymbol{\omega}_p^T \boldsymbol{e}_r \tag{32}$$

4. Design of the Uncertainty and Disturbance Estimator

The estimation laws in Eqs. (16) and (17) are explained in this section. By the definition of $\boldsymbol{\Delta}_{\perp,j}$ and $\boldsymbol{\Delta}_{\parallel,j}$, we know that $\boldsymbol{\Delta}_{\parallel,j}$ will not affect the cable rotational motion as $\boldsymbol{B}_j^T \boldsymbol{\Delta}_{\parallel,j} = \boldsymbol{0}$. If we only examine the cable swing dynamics in Σ_p from Eq. (2) corresponding to the rows block of $\boldsymbol{M}$ block in Eq. (4), we have the following dynamics for cable acceleration:

$$\begin{aligned} m_j \boldsymbol{B}_j^T \Big(\dot{\boldsymbol{v}}_p - \boldsymbol{R}_{IP} \boldsymbol{t}_j^\times \dot{\boldsymbol{\omega}}_p + \boldsymbol{B}_j \dot{\boldsymbol{v}}_j - \boldsymbol{R}_{IP} \boldsymbol{\omega}_p^\times \boldsymbol{t}_j^\times \boldsymbol{\omega}_p + \dot{\boldsymbol{B}}_j \boldsymbol{v}_j\Big) \\ = \boldsymbol{B}_j^T (\boldsymbol{f}_{L,j} + m_j \boldsymbol{g}_I + \boldsymbol{\Delta}_j) = \boldsymbol{B}_j^T (\boldsymbol{f}_{L,j} + m_j \boldsymbol{g}_I + \boldsymbol{\Delta}_{\perp,j}) \end{aligned} \tag{33}$$

The inertial velocity of each quadrotor $\boldsymbol{v}_{q,j}$ is $\boldsymbol{v}_{q,j} = \boldsymbol{v}_p - \boldsymbol{R}_{IP} \boldsymbol{t}_j^\times \boldsymbol{\omega}_p + \boldsymbol{B}_j \boldsymbol{v}_j$ obtained from Ref. [12]. From Eq. (7), we know that $\hat{\boldsymbol{\Delta}}_{\perp,j} = (\boldsymbol{1} - \boldsymbol{L}_j \boldsymbol{L}_j^T / l^2) \hat{\boldsymbol{\Delta}}_j$. Then the estimation error of $\boldsymbol{\Delta}_{\perp,j}$ has similar property:

$$\tilde{\boldsymbol{\Delta}}_{\perp,j} = (\boldsymbol{1} - \boldsymbol{L}_j \boldsymbol{L}_j^T / l^2) \tilde{\boldsymbol{\Delta}}_j \tag{34}$$

The dynamics of the estimator is set to

$$\dot{\tilde{\boldsymbol{\Delta}}}_j = \dot{\hat{\boldsymbol{\Delta}}}_j = -\kappa_j \mathfrak{B}_j \tilde{\boldsymbol{\Delta}}_{\perp,j} \tag{35}$$

Note that based on the design procedure in [6,32] and Assumption 1, $\dot{\boldsymbol{\Delta}}_j \approx \boldsymbol{0}$. Hence, the differential form of the estimated disturbance $\hat{\boldsymbol{\Delta}}_j$ is

$$\dot{\hat{\boldsymbol{\Delta}}}_j = -\kappa_j \mathfrak{B}_j (\hat{\boldsymbol{\Delta}}_j - \boldsymbol{\Delta}_j) = \kappa_j \mathfrak{B}_j \Big(m_j \dot{\boldsymbol{v}}_{q,j} - \boldsymbol{f}_{L,j} + m_j \boldsymbol{g}_I - \hat{\boldsymbol{\Delta}}_j\Big) \tag{36}$$

Equation (16) is the integral form of Eq. (36). After obtaining $\hat{\boldsymbol{\Delta}}_{\perp,j}$, we set the error dynamics of the estimators for the effective disturbance force and torque on the payload as low-pass filters of the true disturbances:

$$\dot{\tilde{\boldsymbol{\Delta}}}_T / \lambda_T = -\tilde{\boldsymbol{\Delta}}_T - \sum_{j=1}^{N} \tilde{\boldsymbol{\Delta}}_{\perp,j}; \quad \dot{\tilde{\boldsymbol{\Delta}}}_R / \lambda_R = -\tilde{\boldsymbol{\Delta}}_R - \sum_{j=1}^{N} \boldsymbol{t}_j^\times \boldsymbol{R}_{PI} \tilde{\boldsymbol{\Delta}}_{\perp,j} \tag{37}$$

We can extract the payload translation dynamics from the first row block of $\boldsymbol{M}$ in Eq. (4) as follows:

$$\begin{aligned} \frac{d}{dt}\Big((m_p + M_q)\boldsymbol{v}_p + \boldsymbol{R}_{IP} \boldsymbol{A}^T \boldsymbol{\omega}_p + \sum_{j=1}^{N} m_j \boldsymbol{B}_j \boldsymbol{v}_j\Big) \\ = \boldsymbol{\Delta}_T + (m_p + M_q)\boldsymbol{g}_I + \sum_{j=1}^{N} (\boldsymbol{f}_{L,j} + \boldsymbol{\Delta}_{\perp,j}) \end{aligned} \tag{38}$$

According to Assumption 1, the derivative of the estimation error becomes

$$\dot{\tilde{\boldsymbol{\Delta}}}_T / \lambda_T = -\tilde{\boldsymbol{\Delta}}_T - \sum_{j=1}^{N} \tilde{\boldsymbol{\Delta}}_{\perp,j}; \quad \dot{\tilde{\boldsymbol{\Delta}}}_T / \lambda_T = \Big(\dot{\hat{\boldsymbol{\Delta}}}_T - \dot{\boldsymbol{\Delta}}_T\Big) / \lambda_T = \dot{\hat{\boldsymbol{\Delta}}}_T / \lambda_T \tag{39}$$

Hence, the error dynamics of $\dot{\hat{\boldsymbol{\Delta}}}_T$ becomes the following:

$$-\tilde{\boldsymbol{\Delta}}_T = \dot{\hat{\boldsymbol{\Delta}}}_T / \lambda_T + \sum_{j=1}^{N} \tilde{\boldsymbol{\Delta}}_{\perp,j} \tag{40}$$

By inserting Eq. (40) into Eq. (38), we have the following update law:

$$\begin{aligned} & \frac{d}{dt}\Big((m_p + M_q)\boldsymbol{v}_p + \boldsymbol{R}_{IP} \boldsymbol{A}^T \boldsymbol{\omega}_p + \sum_{j=1}^{N} m_j \boldsymbol{B}_j \boldsymbol{v}_j\Big) \\ & = \hat{\boldsymbol{\Delta}}_T - \tilde{\boldsymbol{\Delta}}_T + (m_p + M_q)\boldsymbol{g}_I + \sum_{j=1}^{N} (\boldsymbol{f}_{L,j} + \boldsymbol{\Delta}_{\perp,j}) \\ & = \hat{\boldsymbol{\Delta}}_T + \frac{\dot{\hat{\boldsymbol{\Delta}}}_T}{\lambda_T} + (m_p + M_q)\boldsymbol{g}_I + \sum_{j=1}^{N} \Big(\boldsymbol{f}_{L,j} + \boldsymbol{\Delta}_{\perp,j} + \tilde{\boldsymbol{\Delta}}_{\perp,j}\Big) \\ & = \hat{\boldsymbol{\Delta}}_T + \frac{\dot{\hat{\boldsymbol{\Delta}}}_T}{\lambda_T} + (m_p + M_q)\boldsymbol{g}_I + \sum_{j=1}^{N} \Big(\boldsymbol{f}_{L,j} + \hat{\boldsymbol{\Delta}}_{\perp,j}\Big) \end{aligned} \tag{41}$$

Hence, the differential form of the estimator is

$$\begin{aligned} \frac{\dot{\hat{\boldsymbol{\Delta}}}_T}{\lambda_T} = & \frac{d}{dt}\Big((m_p + M_q)\boldsymbol{v}_p + \boldsymbol{R}_{IP} \boldsymbol{A}^T \boldsymbol{\omega}_p + \sum_{j=1}^{N} m_j \boldsymbol{B}_j \boldsymbol{v}_j\Big) - \hat{\boldsymbol{\Delta}}_T \\ & - (m_p + M_q)\boldsymbol{g}_I - \sum_{j=1}^{N} \Big(\boldsymbol{f}_{L,j} + \hat{\boldsymbol{\Delta}}_{\perp,j}\Big) \end{aligned} \tag{42}$$

It is trivial to verify that the integral form of Eq. (42) is equivalent to Eq. (17). Following the same routine, we insert Eq. (37) into the second row block of $\boldsymbol{M}$ to obtain the payload attitude dynamics:

$$\begin{aligned} & \boldsymbol{A} \boldsymbol{R}_{PI} \dot{\boldsymbol{v}}_p + (\boldsymbol{J}_p + \boldsymbol{J}_q) \dot{\boldsymbol{\omega}}_p + \boldsymbol{\omega}_p^\times \boldsymbol{J}_p \boldsymbol{\omega}_p \\ & + \sum_{j=1}^{N} m_j \boldsymbol{t}_j^\times \Big(-\boldsymbol{\omega}_p^\times \boldsymbol{t}_j^\times \boldsymbol{\omega}_p + \boldsymbol{R}_{PI} \boldsymbol{B}_j \dot{\boldsymbol{v}}_j + \boldsymbol{R}_{PI} \dot{\boldsymbol{B}}_j \boldsymbol{v}_j\Big) \\ & = \boldsymbol{\Delta}_R + \sum_{j=1}^{N} \boldsymbol{t}_j^\times \boldsymbol{R}_{PI} (m_j \boldsymbol{g}_I + \boldsymbol{f}_{L,j} + \boldsymbol{\Delta}_{\perp,j}) \end{aligned} \tag{43}$$

Similar to the effective disturbance force, the estimation error has the following property:

$$\begin{aligned} \dot{\tilde{\boldsymbol{\Delta}}}_R / \lambda_R = -\tilde{\boldsymbol{\Delta}}_R - \sum_{j=1}^{N} \boldsymbol{t}_j^\times \boldsymbol{R}_{PI} \tilde{\boldsymbol{\Delta}}_{\perp,j}; \\ \Big(\dot{\hat{\boldsymbol{\Delta}}}_R - \dot{\boldsymbol{\Delta}}_R\Big) / \lambda_R = -\hat{\boldsymbol{\Delta}}_R + \boldsymbol{\Delta}_R - \sum_{j=1}^{N} \boldsymbol{t}_j^\times \boldsymbol{R}_{PI} \tilde{\boldsymbol{\Delta}}_{\perp,j} \end{aligned} \tag{44}$$

Hence we have the following for the dynamics of $\dot{\hat{\boldsymbol{\Delta}}}_R$:

$$\boldsymbol{\Delta}_R = \dot{\hat{\boldsymbol{\Delta}}}_R/\lambda_R + \hat{\boldsymbol{\Delta}}_R + \sum_{j=1}^{N} \boldsymbol{t}_j^{\times} \boldsymbol{R}_{PI} \tilde{\boldsymbol{\Delta}}_{\perp,j} \tag{45}$$

Substituting Eq. (45) into Eq. (43), we have following update law for $\hat{\boldsymbol{\Delta}}_R$:

$$\begin{aligned} &\boldsymbol{A}\boldsymbol{R}_{PI}\dot{\boldsymbol{v}}_p + (\boldsymbol{J}_p + \boldsymbol{J}_q)\dot{\boldsymbol{\omega}}_p + \boldsymbol{\omega}_p^{\times}\boldsymbol{J}_p\boldsymbol{\omega}_p \\ &\quad + \sum_{j=1}^{N} m_j \boldsymbol{t}_j^{\times}\Big(-\boldsymbol{\omega}_p^{\times}\boldsymbol{t}_j^{\times}\boldsymbol{\omega}_p + \boldsymbol{R}_{PI}\boldsymbol{B}_j\dot{\boldsymbol{v}}_j + \boldsymbol{R}_{PI}\dot{\boldsymbol{B}}_j\boldsymbol{v}_j\Big) \\ &= \dot{\hat{\boldsymbol{\Delta}}}_R/\lambda_R + \hat{\boldsymbol{\Delta}}_R + \sum_{j=1}^{N} \boldsymbol{t}_j^{\times}\boldsymbol{R}_{PI}\tilde{\boldsymbol{\Delta}}_{\perp,j} + \sum_{j=1}^{N} \boldsymbol{t}_j^{\times}\boldsymbol{R}_{PI}(m_j\boldsymbol{g}_I + \boldsymbol{f}_{L,j} + \boldsymbol{\Delta}_{\perp,j}) \\ &= \dot{\hat{\boldsymbol{\Delta}}}_R/\lambda_R + \hat{\boldsymbol{\Delta}}_R + \sum_{j=1}^{N} \boldsymbol{t}_j^{\times}\boldsymbol{R}_{PI}\Big(m_j\boldsymbol{g}_I + \boldsymbol{f}_{L,j} + \hat{\boldsymbol{\Delta}}_{\perp,j}\Big) \end{aligned} \tag{46}$$

To avoid using the accelerations of the payload and the cable motion, we use integration by parts to circumvent the unavailable $\dot{\boldsymbol{v}}_p$, $\dot{\boldsymbol{\omega}}_p$, and $\dot{\boldsymbol{v}}_j$ feedback:

$$\begin{aligned} \int \boldsymbol{A}\boldsymbol{R}_{PI}\dot{\boldsymbol{v}}_p\,\mathrm{d}\tau &= \boldsymbol{A}\boldsymbol{R}_{PI}\boldsymbol{v}_p - \int \mathrm{d}(\boldsymbol{A}\boldsymbol{R}_{PI})\boldsymbol{v}_p \\ &= \boldsymbol{A}\boldsymbol{R}_{PI}\boldsymbol{v}_p + \int \boldsymbol{A}\boldsymbol{\omega}_p^{\times}\boldsymbol{R}_{PI}\boldsymbol{v}_p\,\mathrm{d}\tau \end{aligned} \tag{47}$$

$$\begin{aligned} \int \boldsymbol{R}_{PI}(\boldsymbol{B}_j\dot{\boldsymbol{v}}_j)\,\mathrm{d}\tau &= \boldsymbol{R}_{PI}\boldsymbol{B}_j\boldsymbol{v}_j - \int \mathrm{d}(\boldsymbol{R}_{PI})\boldsymbol{B}_j\boldsymbol{v}_j \\ &= \boldsymbol{R}_{PI}\boldsymbol{B}_j\boldsymbol{v}_j + \int \boldsymbol{\omega}_p^{\times}\boldsymbol{R}_{PI}\boldsymbol{B}_j\boldsymbol{v}_j\,\mathrm{d}\tau \end{aligned} \tag{48}$$

5. Time Derivative of V

The total time derivative of V can be obtained by summing all the terms up. Combining Eqs. (29), (31), (32), and (49), we give the result of $\dot{V}$ with Lemma 1 (v). Define a vector $\boldsymbol{u}_K$ as

$$\begin{aligned} \boldsymbol{u}_K &= \begin{bmatrix} \boldsymbol{u}_p^T & \boldsymbol{u}_r^T & \|\tilde{\boldsymbol{r}}_j\| & \|\boldsymbol{\Phi}_j\| & \boldsymbol{u}_{\boldsymbol{\Delta}}^T \end{bmatrix}^T; \\ \boldsymbol{u}_p &= \begin{bmatrix} \|\boldsymbol{e}_{v,i}\| & \|\boldsymbol{e}_{p,i}\| & \|\boldsymbol{R}_1\| & \|\boldsymbol{F}_1\| \end{bmatrix}^T; \\ \boldsymbol{u}_r &= \begin{bmatrix} \|\boldsymbol{\omega}_p\| & \|\boldsymbol{e}_r\| & \|\mathcal{R}_2\| & \|\boldsymbol{\mathcal{F}}_2\| \end{bmatrix}^T; \\ \boldsymbol{u}_{\boldsymbol{\Delta}} &= \begin{bmatrix} \|\tilde{\boldsymbol{\Delta}}_T\| & \|\tilde{\boldsymbol{\Delta}}_R\| & \|\tilde{\boldsymbol{\Delta}}_{\perp,j}\| \end{bmatrix}^T \end{aligned} \tag{50}$$

A symmetric matrix $\boldsymbol{H}_{K,j}$ is constructed as

$$\boldsymbol{H}_{K,j} = \begin{bmatrix} \boldsymbol{H}_P & \boldsymbol{H}_{PA} & \boldsymbol{H}_{rP} & \boldsymbol{0} \\ \star & \boldsymbol{H}_A & \boldsymbol{H}_{rA} & \boldsymbol{H}_{\Phi A} \\ \star & \star & k_L G_{r,j} & \boldsymbol{0} \\ \star & \star & \star & K_0/a_j \end{bmatrix} \tag{51}$$

where $\star$ means that the matrix is symmetric and the element is the transpose of the one on the other side of the diagonal. Sub-blocks of $\boldsymbol{H}_{K,j}$ are defined as follows:

$$\boldsymbol{H}_P = m_p \begin{bmatrix} k_p & 0 & -(k_v + k_p)/2 & -k_p/2 \\ 0 & k_p k_v^2 & -k_p k_v/2 & -k_p k_v/2 \\ \star & \star & k_{r1} & 0 \\ \star & \star & \star & \lambda_1 k_{F1} \end{bmatrix} \tag{52}$$

$$\boldsymbol{H}_A = \begin{bmatrix} k_\Omega & -k_r\delta_\omega\|\boldsymbol{J}_p\|/2 & -(k_\Omega\|\boldsymbol{J}_p^{-1/2}\| + k_r\|\boldsymbol{J}_p^{1/2}\|)/2 & -(k_\Omega\|\boldsymbol{J}_p^{-1/2}\| + \|\boldsymbol{J}_p^{-1/2}\|\cdot\|\boldsymbol{J}_p\|\delta_\omega + \Xi_2\sigma_j\delta_R l)/2 \\ \star & k_r k_\Omega^2 & -k_\Omega k_r\|\boldsymbol{J}_p^{-1/2}\|/2 & -k_r k_\Omega\|\boldsymbol{J}_p^{-1/2}\|/2 \\ \star & \star & k_{r2} & 0 \\ \star & \star & \star & \lambda_2 k_{F2} \end{bmatrix} \tag{53}$$

The final integral form of $\hat{\boldsymbol{\Delta}}_R$ without the acceleration feedback based on Eqs. (47) and (48) is in Eq. (17).

Proposition 3: Hence, according to Eqs. (36), (40), (45) and Lemma 1 (iv), the time derivative of V_4 can be obtained as

$$\dot{V}_4 \le -\sum_{j=1}^{N} a_j\left[\frac{1}{2}\lambda_T c_T \tilde{\boldsymbol{\Delta}}_T^2 + \frac{1}{2}\lambda_R c_R \tilde{\boldsymbol{\Delta}}_R^2 + c_j\kappa_j\tilde{\boldsymbol{\Delta}}_{\perp,j}^2\right] \le 0 \tag{49}$$

Proof: See Appendix C.

Remark 2: $\dot{V}_4 \le 0$ means that $0 \le V_4(t) \le V_4(0)$, $\forall t > 0$. If $\boldsymbol{0}$ is picked as the initial value for each estimator, we have $V_4(0) = (1/2)c_T\boldsymbol{\Delta}_T^2 + (1/2)c_R\boldsymbol{\Delta}_R^2 + (1/2)\sum_{j=1}^{N}((a_j c_R\lambda_R N^2\Gamma_c^2 + c_T\lambda_T N)/(2\kappa_j) + c_j a_j)\boldsymbol{\Delta}_j^2$. $V_4(0)$ is determined by the magnitude of all the disturbances. According to Assumption 1, $V_4(0)$ is bounded. Therefore, $\forall t > 0$, $\|\tilde{\boldsymbol{\Delta}}_T\| \le \sqrt{2V_4(t)/c_T} \le \sqrt{2V_4(0)/c_T}$, $\|\tilde{\boldsymbol{\Delta}}_R\| \le \sqrt{2V_4(t)/c_R} \le \sqrt{2V_4(0)/c_R}$, and $\|\tilde{\boldsymbol{\Delta}}_{\perp,j}\| \le \|\tilde{\boldsymbol{\Delta}}_j\| \le \sqrt{2V_4(0)/((a_j c_R\lambda_R N^2\Gamma_c^2 + c_T\lambda_T N)/(2\kappa_j) + a_j c_j)}$. Hence all estimation errors are bounded for the closed-loop system by design, which is an advantage of the UDE technique compared with adaptive control. Hence according to (A18), $\|\hat{\boldsymbol{b}}_j\| \le \|\boldsymbol{b}_j\| + \|\tilde{\boldsymbol{b}}_j\| \le \|\boldsymbol{\Delta}_T\| + E_0\|\boldsymbol{\Delta}_R\| + \sqrt{2V_4(0)/c_T} + E_0\sqrt{2V_4(0)/c_R}$. Therefore, if all disturbances are bounded such that $\|\tilde{\boldsymbol{b}}_j\| \le \epsilon m_p g$ (with $\epsilon < 1$), β_j is bounded, and finally $h_{\delta,j}$ is bounded.

$$\boldsymbol{H}_{rP} = \begin{bmatrix} 0 \\ 0 \\ -m_p\gamma_j\Xi_1 k_{r1}/2 \\ -m_p\Xi_1(\lambda_1\gamma_j + \delta_r k_L)/2 \end{bmatrix}; \quad \boldsymbol{H}_{rA} = \begin{bmatrix} -\gamma_j\|\boldsymbol{E}_j\boldsymbol{\Delta}_R\|/2 \\ 0 \\ -\gamma_j\Xi_2\sigma_j k_{r2}/2 \\ -\Xi_2\sigma_j(\delta_r k_L + \gamma_j\lambda_2 + \delta_\omega\gamma_j)/2 \end{bmatrix} \tag{54}$$

$$\boldsymbol{H}_{PA} = \begin{bmatrix} 0 & 0 & 0 & 0 \\ 0 & 0 & 0 & 0 \\ 0 & 0 & 0 & 0 \\ -m_p\Xi_1\delta_R l/2 & 0 & 0 & 0 \end{bmatrix}; \quad \boldsymbol{H}_{\boldsymbol{\Phi}A} = \begin{bmatrix} -m_j k_L l\delta_r\delta_R/(2a_j) \\ 0 \\ 0 \\ 0 \end{bmatrix};$$

$$\boldsymbol{H}_{\delta,j} = -\begin{bmatrix} h_{\delta,j}/a_j + 1 \\ E_0(h_{\delta,j}/a_j + 1) \\ 1/a_j \end{bmatrix}^T \Big/ 2 \tag{55}$$

$$
\boldsymbol{H}_{\boldsymbol{\Delta},j} = \begin{bmatrix} \lambda_T c_T/2 & 0 & 0 \\ 0 & \lambda_R c_R/2 & 0 \\ 0 & 0 & \kappa_j c_j \end{bmatrix}; \quad \boldsymbol{H}_{K,\boldsymbol{\Delta}} = \begin{bmatrix} \boldsymbol{0}_{4\times 3} \\ \boldsymbol{0}_{4\times 3} \\ \boldsymbol{0}_{1\times 3} \\ \boldsymbol{H}_{\delta,j} \end{bmatrix} \tag{56}
$$

The final form of $\dot{V}$ is as follows:

$$
\dot{V} \leq -\sum_{j=1}^{N} a_j \boldsymbol{u}_K^T \begin{bmatrix} \boldsymbol{H}_{K,j} & \boldsymbol{H}_{K,\boldsymbol{\Delta}} \\ \boldsymbol{H}_{K,\boldsymbol{\Delta}}^T & \boldsymbol{H}_{\boldsymbol{\Delta},j} \end{bmatrix} \boldsymbol{u}_K \tag{57}
$$

Remark 3: From Eq. (52), if k_{r1} and $\lambda_1 k_{F1}$ are significantly larger than k_v and k_p, matrix $\boldsymbol{H}_P$ is positive definite because its diagonal blocks are positive definite and the off-diagonal blocks only contain k_v and k_p. Following the similar routine, we can pick k_{r2}, $\lambda_2 k_{F2}$, k_r, and k_Ω such that $\boldsymbol{H}_A$ is positive definite. Since $G_{r,j}$ and K_0 only appear in the diagonal of $\boldsymbol{H}_{K,j}$, $\boldsymbol{H}_{K,j}$ can be positive definite if δ_R in $\boldsymbol{H}_{PA}$ and $\boldsymbol{H}_{\Phi A}$ are small enough. From Eq. (57), since $h_{\delta,j}$ is bounded, we can pick c_T, c_R, and c_j high enough so that $\dot{V}$ is negative definite if $\boldsymbol{H}_{K,j}$ is positive definite. Since c_T, c_R, and c_j are only used in the stability analysis, and $h_{\delta,j}$ is bounded, we do not need to calculate their actual values. From Eq. (57), we can see that all path-following errors are zero when $\dot{V} = 0$. It is essential to emphasize that the closed-loop system is autonomous since time is not explicitly expressed in the control law by the problem formulation. According to the LaSalle's theorem, we can conclude that the path-following control based on the virtual control force is AS.

C. Stability of the Complete System

Let $\boldsymbol{\rho}_j = -\boldsymbol{R}_{Ij}\boldsymbol{e}_3\|\boldsymbol{f}_{v,j}\| - \boldsymbol{f}_{v,j}$ denote the error between the desired and the actual lift. According to [33], the attitude tracker is exponentially stable, so there exists a subset of its domain of attraction denoted as $\mathbb{D}_r$ such that $\boldsymbol{\rho}_j \to \boldsymbol{0}$ as $t \to \infty$ and $\|\boldsymbol{\rho}_j(t)\| < \|\boldsymbol{\rho}_j(0)\|$. Then based on the bound in Remark 1, a sublevel set $\mathbb{D}_v$ associated with $V(\mathcal{X})$ becomes

$$
D = \left\{ \mathcal{X} | \|\boldsymbol{\omega}_p\| \leq \delta_\omega, \|\boldsymbol{r}_j\|/l \leq \sqrt{1 - 1/\delta_r^2}; \right.
$$

$$
\left. \|\boldsymbol{v}_j\|/l \leq \delta_v, \boldsymbol{e}_3^T \boldsymbol{f}_{v,j} < 0, \quad \|\hat{\boldsymbol{b}}_j\| \leq \epsilon m_p g \right\}
$$

$$
\mathbb{D}_v = \{ \mathcal{X} | V(\mathcal{X}) \leq c^\star \}; \qquad c^\star = \min_{X \in \partial D} V \tag{58}
$$

If $\|\boldsymbol{\rho}_j(0)\| \leq \epsilon_\phi \|\boldsymbol{\Phi}_j(\mathcal{X}(0))\|$, $\mathcal{X}(0) \in \mathbb{D}_v$, where $(K_0 - \min_{\dot{V} \leq 0} K_0)/2 > \epsilon_\phi > 0$, then $\dot{V} < 0$, meaning that all trajectories of the closed-loop system starting in $\mathbb{D}_v$ stay in $\mathbb{D}_v$. Therefore, an estimated domain of attraction is $\mathbb{D} = \{\mathcal{X} | \mathcal{X}_p \in \mathbb{D}_v, \mathcal{X}_{\mathrm{rot}} \in \mathbb{D}_r, \dot{V}(0) + \sum_{j=1}^{N} \|\boldsymbol{\Phi}_j(0)\| \cdot \|\boldsymbol{\rho}_j(0)\| \leq 0\}$. According to the reduction theorem in Theorems 6 and 10 of Ref. [33], if the inner loop is AGAS and the outer loop is AS, it is trivial to show that the complete system is AS. A detailed explanation is provided in Sec. IV.C.3 of Ref. [31]. The conclusion is summarized in the following theorem:

Theorem 1 (stability of Σ under the proposed control law): Given system Σ and a path $\mathbb{P}$, if the following conditions are met then the complete system Σ is asymptotically stable under the virtual control in Eq. (15):

1) Configuration requirements in Eq. (11) are met.

2) The initial condition of the system is within an estimated domain of attraction of $\mathbb{D}$.

3) Parameters are picked such that $\boldsymbol{H}_{K,j}$ defined in Eq. (57) is positive definite.

4) The inequality in Eq. (26) holds such that the Lyapunov function is positive definite.

5) An AGAS attitude tracker is used such as the one in Eq. (20).

Remark 4: It is crucial to point out that Theorem 1 is only a sufficient condition to achieve asymptotic stability. The estimated domain of attraction and parameters satisfying Eq. (57) may be conservative in terms of performance. Therefore, the baseline gains from Eq. (57) such as k_v and k_r could be increased to get better performance. The increased gains may violate parameter constraints, so the stability of the system with increased gains needs to be tested by additional simulation and experiments.

V. Simulations

A slung-load transportation simulation is presented to show the performance of the controller when traveling on a large-scale path with a variety of strong external disturbances, as a complementary to the flight test results in the next section. The slung load is carried by three drones with their parameters shown in Table 1. The controller parameters are listed in Table 2. The parameters in Tables 1 and 2 satisfy the conditions in Theorem 1. A path consisting four segments was used in simulation with parameter listed in Table 3. The reference position and velocity on the arc segment are defined as $\boldsymbol{n}_r = (\boldsymbol{x}_p - \boldsymbol{x}_c)/\|\boldsymbol{x}_p - \boldsymbol{x}_c\|$, where $\boldsymbol{n}_c = -\boldsymbol{n}_r^\times \boldsymbol{e}_3/\|\boldsymbol{n}_r^\times \boldsymbol{e}_3\|$. The reference position and velocity are $\boldsymbol{p}_c = \boldsymbol{x}_p - R\boldsymbol{n}_r - \boldsymbol{x}_c$ and $\boldsymbol{v}_c = \boldsymbol{n}_c w_c$, respectively. Here $\boldsymbol{x}_c = [85 \quad 23 \quad -10]^T$ m is the center of the arc;

Table 1 System parameters

Parameter	Description	Value
m_j	Quadrotor mass	1.63 kg
m_p	Payload mass	1.30 kg
$\boldsymbol{J}_j$	Quadrotor moment of inertia	diag ([0.1 0.1 0.3]) kg · m^2
$\boldsymbol{J}_p$	Payload moment of inertia	diag ([5 5 5]) × 10^{-1} kg · m^2
$\boldsymbol{t}_1$	1st tether point	$[1.085 \quad 0 \quad 0]^T$ m
$\boldsymbol{t}_2$	2nd tether point	$[-0.5425 \quad -0.9396 \quad 0]^T$ m
$\boldsymbol{t}_3$	3rd tether point	$[-0.5425 \quad 0.9396 \quad 0]^T$ m
L	Cable length	0.98 m

Table 2 Control parameters

Parameter	Value
K_0	6.0
k_L	0.15
k_v	0.24
k_p	0.10
b_r	0.5
k_{r1}	0.2
k_Ω	0.10
k_r	0.055
k_{r2}	0.2
b_ω	2.0
λ_1	0.4
λ_2	0.4
λ_T	0.1
λ_R	0.2
κ_j	1.0
a_1, a_2, a_3	0.3333
K_0(experiment)	diag ([6.0 6.0 9.0])
k_r(experiment)	diag ([0.055 0.055 0.15])
k_v(experiment)	diag ([0.24 0.24 0.7])

Table 3 Trajectory parameters

Waypoint location, m	Direction	Velocity, m/s
$\boldsymbol{P}_1 = [0 \quad 3 \quad -10]^T$	$\boldsymbol{n}_1 = [1 \quad 0 \quad 0]^T$	$w_1 = 3$
$\boldsymbol{P}_2 = [105 \quad 23 \quad -10]^T$	$\boldsymbol{n}_2 = [0 \quad 1 \quad 0]^T$	$w_2 = 3$
$\boldsymbol{P}_3 = [105 \quad 83 \quad -10]^T$	$\boldsymbol{n}_3 = [-0.98 \quad -0.20 \quad -0.10]^T$	$w_3 = 3$

Table 4 External disturbances

Disturbances on the payload	Disturbance forces on each drone
$\boldsymbol{\Delta}_t = [0.2 \quad -0.1 \quad 0.3]^T$ m	$\boldsymbol{\Delta}_1 = [0.1 \quad 0.2 \quad 0.3]^T$ N
$\boldsymbol{\Delta}_r = [-0.3 \quad 0.25 \quad 0.2]^T$ N · m	$\boldsymbol{\Delta}_2 = [-0.1 \quad -0.1 \quad 0.25]^T$ N
$\boldsymbol{\Delta}_{t,s} = 0.2\sin(0.4t)\cdot[1.0 \quad 1.0 \quad 1.0]^T$ N	$\boldsymbol{\Delta}_3 = [-0.3 \quad 0.3 \quad -0.15]^T$ N
$\boldsymbol{\Delta}_{r,s} = 0.1\sin(0.2t)\cdot[1 \quad 1 \quad 1]^T$ N · m	$\boldsymbol{\Delta}_{1,s} = 0.2\sin(0.4t)\cdot[1 \quad 1 \quad 1]^T$ N
$\boldsymbol{\Delta}_I = [0 \quad 5 \quad 0]^T$ N	$\boldsymbol{\Delta}_{2,s} = 0.2\sin(0.4t + 2\pi/3)\cdot[1 \quad 1 \quad 1]^T$ N
——	$\boldsymbol{\Delta}_{3,s} = 0.2\sin(0.4t + 4\pi/3)\cdot[1 \quad 1 \quad 1]^T$ N

$w_c = 3$ m/s is the reference speed on the circle; $R = 20$ m is the radius of the arc. When the payload is traveling on the arc segment path, $\boldsymbol{p}_i$ is replaced by $\boldsymbol{p}_c$, and $\boldsymbol{v}_{d,i}$ is replaced by $\boldsymbol{v}_c$ to obtain $\boldsymbol{e}_{p,i}$ and $\boldsymbol{e}_{v,i}$. The initial Euler angles of the payload are $\theta = \psi = 0$ deg and $\phi = 10$ deg. The initial position and velocity of the payload are $\boldsymbol{x}_{p,0} = [55 - 3]^T$ m, $\boldsymbol{v}_{p,0} = \mathbf{0}$ m/s, and $\boldsymbol{\omega}_{p,0} = \mathbf{0}$ rad/s, respectively. The payload target attitude is $\phi = 0$ deg and $\theta = 0$ deg for all segments. The yaw angle commands before and after $\boldsymbol{P}_3$ are $\psi = 0$ deg and $\psi = 90$ deg, respectively. The disturbances are shown in Table 4. The disturbances with subscript s are additional time-varying parts that are only activated from $t = 38$ s to $t = 48$ s. $\boldsymbol{\Delta}_I$ is the impulse activated from $t = 68$ s to $t = 73$ s to simulate strong wind gust. Band-limited white noises were added in the system to simulate random air turbulence. The power and the sample time of the band-limited white noises are 0.000001 $(\mathrm{m/s}^2)^2/\mathrm{Hz}$ and 0.01 s, which result in a $3-\sigma$ boundary of roughly 0.3 N. The total disturbances are the sum of the constant part, the time-varying part, the impulse force part, and the white-noise part.

The path-following results are shown in Fig. 3, where the payload is stabilized onto the given path under external disturbances. The SD ON/OFF and GD ON/OFF marks in Fig. 3 indicate the trajectory segment when the sinusoidal disturbances and impulse disturbances are activated and deactivated, respectively. Snapshots of the payload attitude are given in Fig. 4a. As indicated in Fig. 4b, the path error approaches zero when all external disturbances are nearly constant and the reference trajectories are straight lines. When the payload is traveling on the arc segment path or the sinusoidal disturbances are activated, the controller can stabilize the payload close to the given path. To test the capability of the controller under abrupt path segment switching, the turning angle between the segment before and after $\boldsymbol{P}_3$ is greater than 90 deg. The reference attitude is also changed after $\boldsymbol{P}_3$. The spikes at around $t = 55$ s in Fig. 4b are the initial error caused by the segment switching. It can be seen from Figs. 4b and 3 that after the initial jump of the path errors, the controller can still stabilize the payload smoothly to the new path segment.

Figures 5a and 5b show the estimated disturbances and errors. In the presence of the random noise turbulence, the estimation errors converge close to zero. Since the disturbance estimators are low-pass filters, the nonzero estimation errors are caused by the time-varying and random noise on the system. When the impulse force is activated, the estimator is able to compensate for part of the additional disturbance as shown in Figs. 3 and 5a, resulting in a jump in the estimation error. However, the path and disturbance estimation error eventually converge close to zero when the impulse force is turned off.

Figure 6a shows the cable tip motion of the path-following task. The cable motion decays when the payload is on the desired path. Figure 6b provides the lift and the magnitude of the torque generated by each quadrotor. Note that the spikes in the magnitude of the torque are caused by path segment switching and numerical differentiation used in obtaining $\boldsymbol{\omega}_{d,j}$ and $\dot{\boldsymbol{\omega}}_{d,j}$. To sum up, we conclude that the proposed control law is capable of stabilizing the payload on a given reference path under the external disturbances.

VI. Flight Demonstration

Flight demonstrations were performed in the Flight Systems and Control (FSC) OptiTrack Lab shown in Fig. 7b. S500 quadrotors were used as shown in Fig. 7a. The system parameters are listed in Tables 1 and 2. Note that the z component of k_v, k_r, and K_0 are set to 0.7, 0.15, and 9.0, respectively, to reduce the initial height deviation and yaw drifting in the takeoff phase for safety reasons. The pose of the quadrotor and the payload were measured by 14 OptiTrack Flex 13 cameras. The velocity and angular velocity were sent to the Nvidia Jetson Nano computer on each drone via 5G Hz Wi-Fi network at a frequency of 50 Hz. The computer combined the feedback

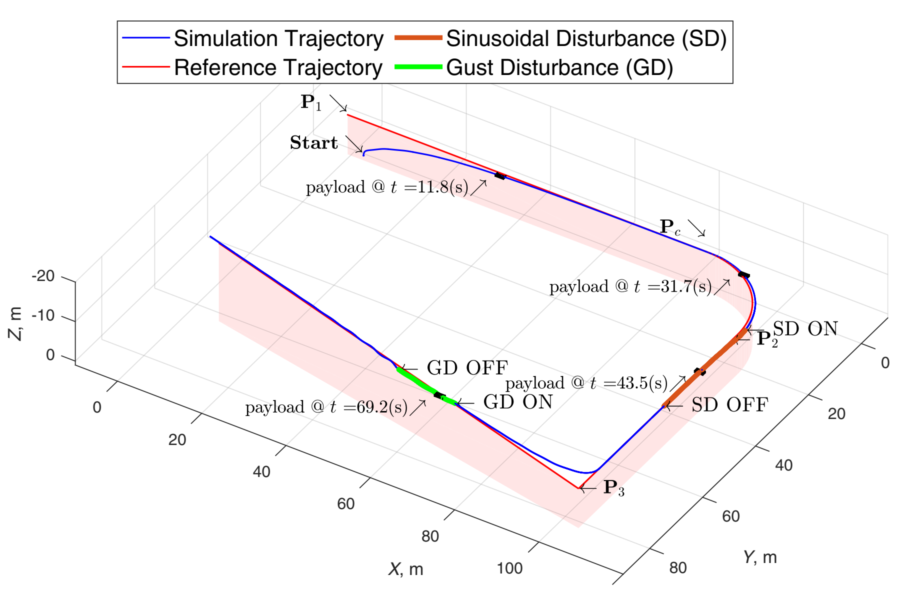

Fig. 3 The trajectory tracking result. SD ON/OFF and GD ON/OFF indicate the trajectory segment when sinusoidal and gust disturbance are activated, respectively.

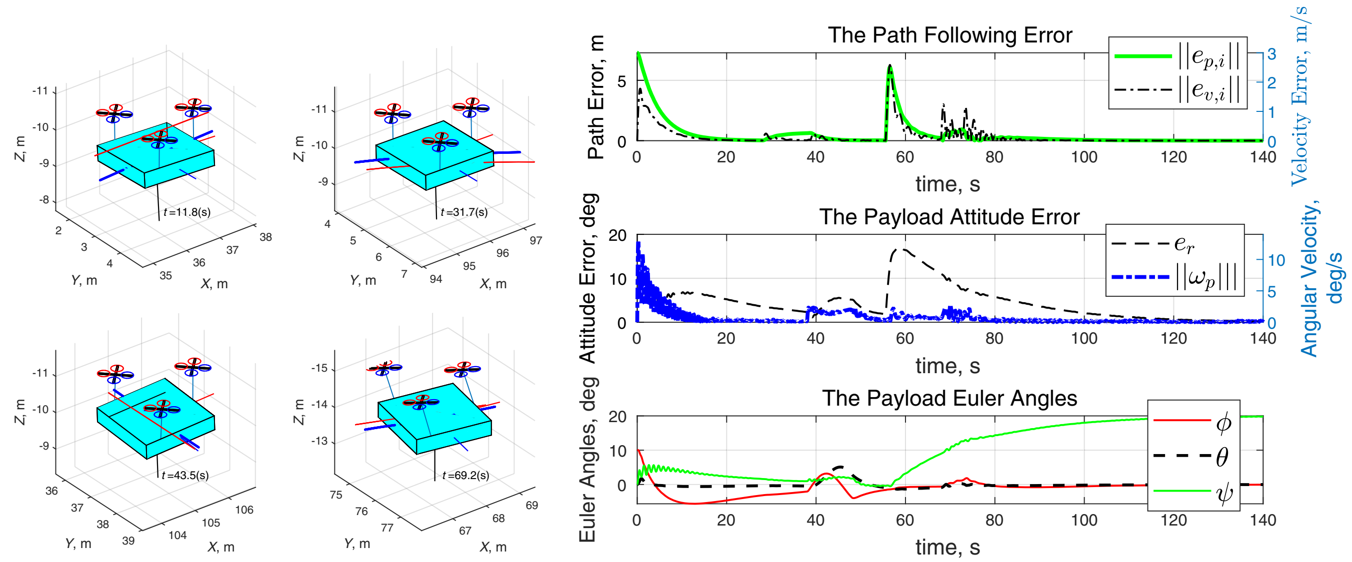

a) The snapshots of the payload attitude

b) The path-following error (Note that the markers of the velocity error e_v and the angular velocity ω_p are on the left side of the plot.)

Fig. 4 Snapshots of the payload attitude at four time stamps and the path-following error.

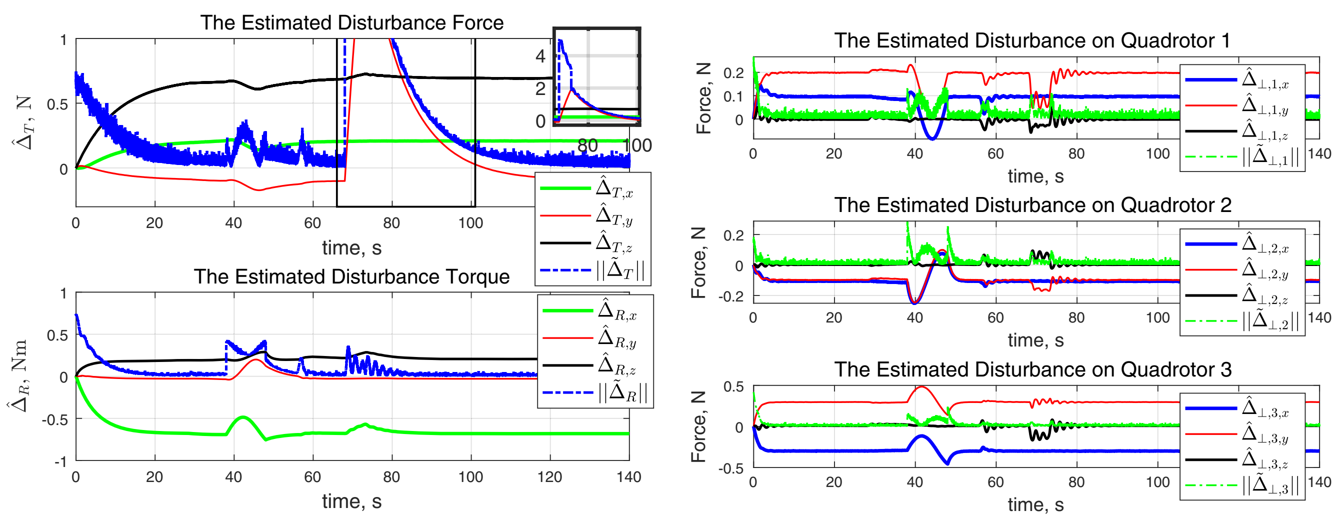

a) The estimated effective disturbances on the payload

b) The estimated effective disturbances on each quadrotor

Fig. 5 Quadrotor relative motion and command lift.

information from Optitrack and IMU to calculate $\boldsymbol{f}_{v,j}$. A Pixhawk 4 flight control unit (FCU) was used to receive the attitude setpoint command via Mavros from the onboard computer to control the speed of each motor in OFFBOARD mode. Robotic operating system (ROS) was used for programming the control and communication algorithms. Native PX4 firmware was used in FCU. Three drones were used in the flight test. Because of limited laboratory space and safety requirements, only position and attitude stabilization tests have been performed. Therefore, the path error is redefined for experiments as $\boldsymbol{e}_{p,i} = \boldsymbol{x}_p - \boldsymbol{x}_t$. We recorded experimental results from three test scenarios. Scenario A and B are position[‡] and attitude stabilization with a platform shaped payload. Scenario C is a parameter uncertainty test,[¶] where a 200 g object is put on the payload platform as an exogenous uncertainty. In Figs. 6, 8, and 10, the states with the subscript t represent the command value sent to the controller.

A. Cooperative Transport Test: Position Stabilization

The position stabilization result is shown in Fig. 6. The x position response of the payload is shown in Fig. 8b. It can be seen that the motion of the payload in x direction follows the command position from -0.3 to 0.6 m while maintaining the attitude angles close to zero. The motion in y and z directions stays close to the equilibrium. The oscillation in the attitude channel is caused by the air turbulence and payload structural flexibility. Figure 9a presents the estimated effective disturbances on the payload. The z component of $\hat{\boldsymbol{\Delta}}_T$ decreases with time because the thrust available drops when the battery voltage drops due to energy draining. The estimated torque on the payload varies from $-0.7\ \mathrm{N \cdot m}$ to $0.4\ \mathrm{N \cdot m}$. This is due to the push of the downwash streams from the propellers. Each drone is slightly different in terms of battery consumption, so the thrust loss due to battery voltage drop is asynchronous, resulting in a net disturbance moment on the payload. Figure 9b shows the estimated disturbance on each quadrotor and the cable tip movement. Note that

[‡]https://www.youtube.com/watch?v=Z9-OlCR-daIlist=PLGJ05aPUKXH-Y6WUyEvXKBSRT5AAzUQf- index=6.

[§]https://www.youtube.com/watch?v=ezC7Rm9ApeIlist=PLGJ05aPUKXH-Y6WUyEvXKBSRT5AAzUQf- index=7.

[¶]https://www.youtube.com/watch?v=LptDhJcvnUglist=PLGJ05aPUKXH-Y6WUyEvXKBSRT5AAzUQf- index=8.

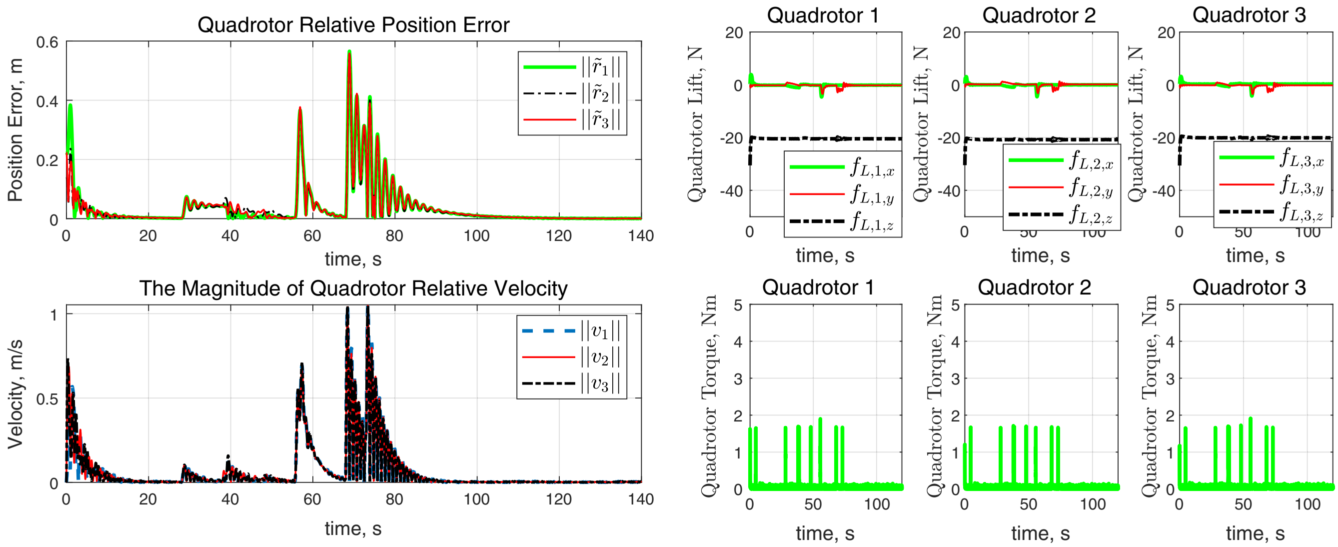

a) The position and velocity of quadrotors relative to the payload
b) The lift and the magnitude of the torque by propellers

Fig. 6 The position command experiment.

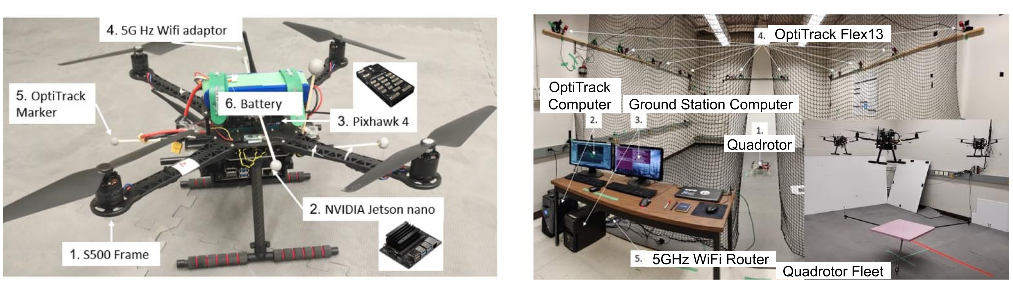

a) S500 quadrotor
b) The layout of FSC OptiTrack room

Fig. 7 The position command experiment: the estimated disturbances and the cable tip motion.

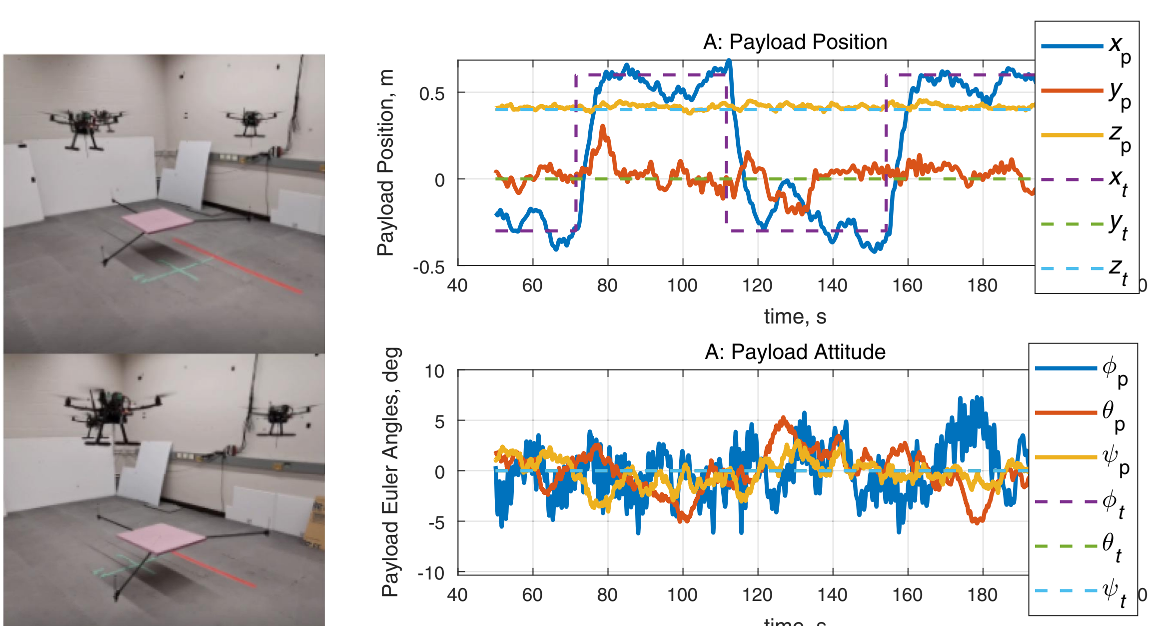

a) The position setpoint test
b)The position and attitude response of the payload

Fig. 8 The attitude command experiment.

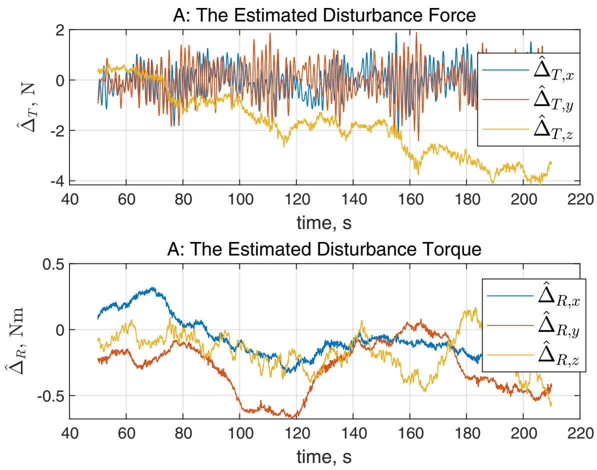

a) The estimated disturbances on the payload

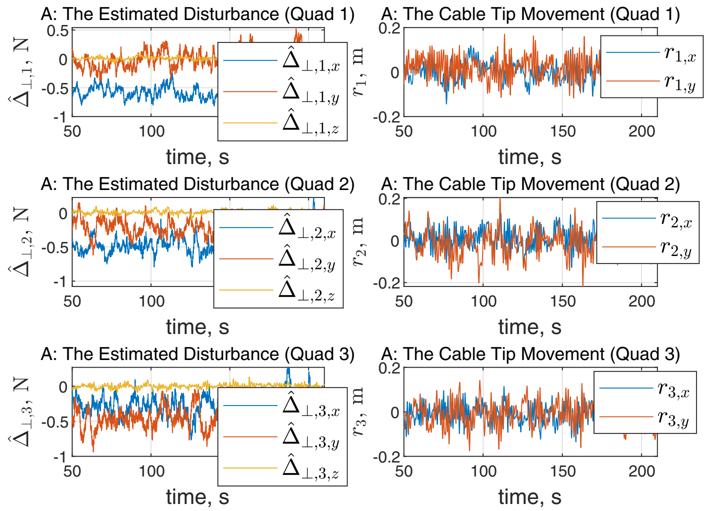

b) The estimated disturbances on each quadrotor and the cable tip motion

Fig. 9 The attitude command experiment: estimated disturbances and the cable tip motion.

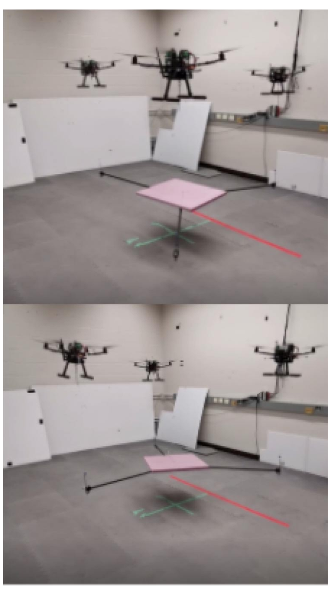

a) The attitude setpoint test

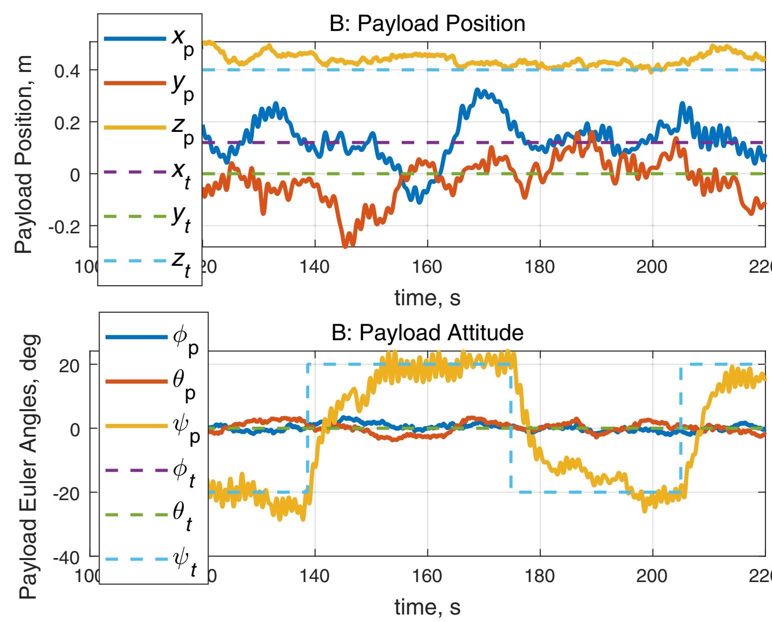

b) The position and attitude response of the payload

Fig. 10 The disturbance rejection experiment.

the estimated disturbances on each drone are not zero. The rotor arms will deform due to structure flexibility. However, the bending angles of arms are not the same, creating an offset in the lift direction. The tilted lift in the body-fixed frame is the primary source of the disturbances on each drone. The cable tip deviations are under 0.1 m for most of the time.

B. Cooperative Transport Test: Attitude Stabilization

The attitude control result is shown in Fig. 8. The slung load revolved around the yaw axis according to a command angle that varied from −20 to 20 deg without steady-state errors. The position deviation from the equilibrium in x and y directions are roughly 0.3 m. There are also high-frequency oscillations in the yaw response. These vibrations are caused by the payload and cable flexibility. From Fig. 10a, there are bars protruding out from the platform that may contribute to the vibration of the slung load. However, the proposed controller can withstand these unmodeled dynamics with decent performance thanks to the disturbance estimator design. Figures 11a and 11b show the estimated disturbances and the cable tip movement of cables. The estimated disturbances resemble similar trend as in case A. The decreasing force in the z direction is a result of battery voltage drop during the flight. Similar to case A, the z component of the $\hat{\boldsymbol{\Delta}}_T$ decreases due to battery consumption. The cable tip deviations are under 0.15 m for most of the time. The results show that the proposed controller is able to manipulate the payload to a given command attitude in the presence of unmodeled dynamics.

C. Cooperative Transport Test: Parameter Uncertainty

The parameter uncertainty tasks are shown in Fig. 10. The subfigures labeled I and II denote the position and attitude command results with an additional object on the platform, respectively. The position command is in the x direction from −0.3 to 0.6 m. The attitude command is in the yaw channel from −20 to 20 deg. From Fig. A1b, the position and the attitude of the payload converge to the command values without steady-state errors, verifying the robustness of the controller. Figure A2a shows the estimated effective

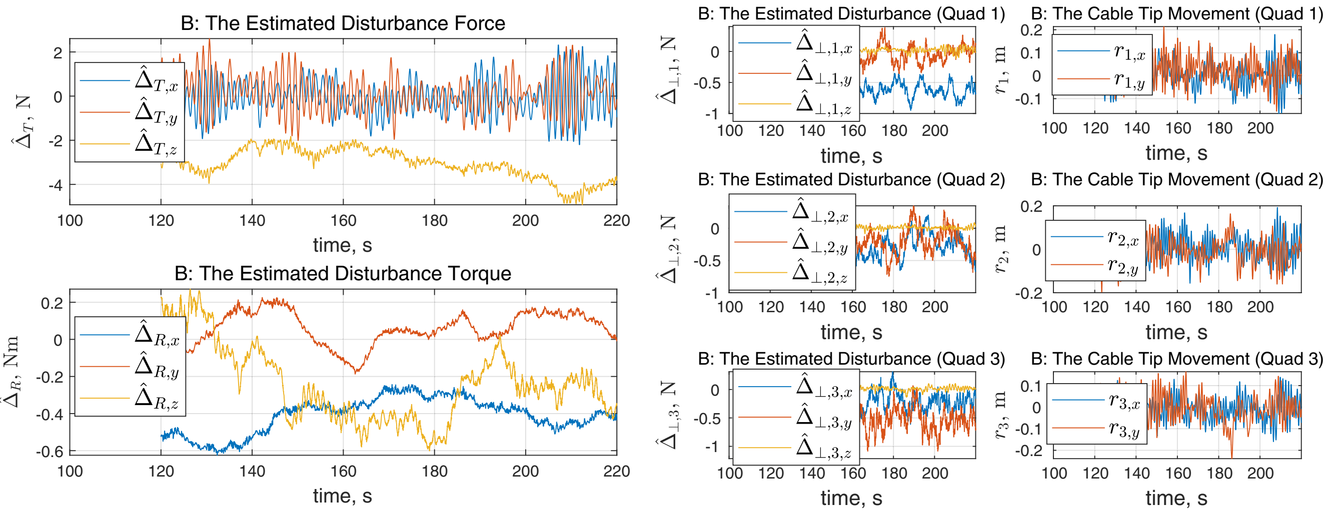

a) The estimated disturbances on the payload

b) The estimated disturbances on each quadrotor and the cable tip motion

Fig. 11 The disturbance rejection experiment: estimated disturbances.

disturbances of the slung load. Similar to the previous cases, the z component of the $\hat{\boldsymbol{\Delta}}_T$ decreases due to battery consumption, and the high-frequency noises are from air turbulence and structural flexibility. Figure A2b presents the estimated disturbances on each quadrotor for the two cases. The nonzero estimations are mainly caused by drone structural deformation. To sum up, the experiment tests show the robustness of the controller under disturbances, and the proposed control law can be used as a potential candidate for cooperative slung-load delivery.

VII. Conclusions

A novel path-following LP controller for multiple quadrotors carrying a slung payload has been described in this paper. The slung load and the carrier vehicles are modeled and controlled as a complete nonlinear multibody system. The PFP problem is then formulated as the payload traveling on the desired path with a desired attitude. A robust path-following controller has been designed based on the idea of UDE. The main novelty of this paper is the design of the virtual controller for the outer loop. With the help of the disturbance estimator, the payload can travel on the given path even in the presence of external disturbances. The attitude controller for each quadrotor is the inner loop. The choice of the attitude controller is independent of the virtual controller, so different robust controllers can be implemented on drones. Stability analysis has been conducted to show that the combination of the virtual controller and the attitude tracker provides an AS system.

A path-following simulation demonstrating the capability of the proposed controller is presented. Even under various time-varying disturbances, the closed-loop system managed to stay around the reference trajectory, which verifies the capability of the proposed controller. If the external disturbances are constants, such as inaccurate mass measurements, the steady-state error reaches zero as time goes to infinity.

Flight tests demonstrate the performance of the proposed approach. Three scenarios were presented: the position command test, the attitude command test, and the disturbance rejection test. The payload reached the desired position and attitude even with an unknown object on the platform. Stable hovering is achieved and the overall performance is verified.

Appendix A: Proof of Proposition 1

By using the passivity of the system, i.e., $\dot{\boldsymbol{M}} - 2\boldsymbol{C}$ is skew symmetric, the time derivative of V_1 is

$$\begin{aligned}\dot{V}_1 &= (\boldsymbol{u}+\boldsymbol{u}_d)^T(\boldsymbol{M}(\dot{\boldsymbol{u}}+\dot{\boldsymbol{u}}_d)+\boldsymbol{C}(\boldsymbol{u}+\boldsymbol{u}_d)) \\ &= (\boldsymbol{u}+\boldsymbol{u}_d)^T(\boldsymbol{F}+\boldsymbol{G}+\boldsymbol{\Delta}+\boldsymbol{M}\dot{\boldsymbol{u}}_d+\boldsymbol{C}\boldsymbol{u}_d)\end{aligned} \tag{A1}$$

$$\boldsymbol{F}+\boldsymbol{G}+\boldsymbol{\Delta} = \begin{bmatrix} (m_p+M_q)\boldsymbol{g}_I + \boldsymbol{\Delta}_T + \sum_{j=1}^N(\boldsymbol{f}_{L,j}+\boldsymbol{\Delta}_{\perp,j}) \\ \boldsymbol{\Delta}_R + \sum_{j=1}^N \boldsymbol{t}_j^\times \boldsymbol{R}_{PI}(\boldsymbol{\Delta}_{\perp,j} + m_j\boldsymbol{g}_I + \boldsymbol{f}_{L,j}) \\ \boldsymbol{B}_1^T(m_1\boldsymbol{g}_I + \boldsymbol{\Delta}_1 + \boldsymbol{f}_{L,1}) \\ \vdots \\ \boldsymbol{B}_N^T(m_N\boldsymbol{g}_I + \boldsymbol{\Delta}_N + \boldsymbol{f}_{L,N}) \end{bmatrix} \tag{A2}$$

Note that according to the configuration property in Eq. (12), the following terms are zero:

$$\begin{cases} \sum_{j=1}^N a_j \boldsymbol{R}_{IP}\boldsymbol{E}_j\boldsymbol{\Delta}_R = \boldsymbol{R}_{IP}\left(\sum_{j=1}^N a_j\boldsymbol{E}_j\right)\boldsymbol{\Delta}_R = \boldsymbol{0} \\ \sum_{j=1}^N \boldsymbol{t}_j^\times \boldsymbol{R}_{PI}(a_j\boldsymbol{\Delta}_T + a_j m_p\boldsymbol{g}_I) = \left(\sum_{j=1}^N a_j\boldsymbol{t}_j^\times\right)\boldsymbol{R}_{PI}(\boldsymbol{\Delta}_T + m_p\boldsymbol{g}_I) = \boldsymbol{0} \end{cases} \tag{A3}$$

Based on Eqs. (A3) and (8), $\boldsymbol{F}+\boldsymbol{G}+\boldsymbol{\Delta}$ can be rearranged to show the effective disturbances explicitly:

$$\boldsymbol{F}+\boldsymbol{G}+\boldsymbol{\Delta} = \begin{bmatrix} \sum_{j=1}^N(\boldsymbol{f}_{L,j}+\boldsymbol{\Delta}_{\perp,j}+a_j\boldsymbol{\Delta}_T+a_j\boldsymbol{R}_{IP}\boldsymbol{E}_j\boldsymbol{\Delta}_R+a_j m_p\boldsymbol{g}_I+m_j\boldsymbol{g}_I) \\ \sum_{j=1}^N \boldsymbol{t}_j^\times\boldsymbol{R}_{PI}(\boldsymbol{f}_{L,j}+\boldsymbol{\Delta}_{\perp,j}+a_j\boldsymbol{\Delta}_T+a_j\boldsymbol{R}_{IP}\boldsymbol{E}_j\boldsymbol{\Delta}_R+a_j m_p\boldsymbol{g}_I+m_j\boldsymbol{g}_I) \\ \boldsymbol{B}_1^T(\boldsymbol{f}_{L,1}+\boldsymbol{\Delta}_{\perp,1}+m_1\boldsymbol{g}_I) \\ \vdots \\ \boldsymbol{B}_N^T(\boldsymbol{f}_{L,N}+\boldsymbol{\Delta}_{\perp,N}+m_N\boldsymbol{g}_I) \end{bmatrix} \tag{A4}$$

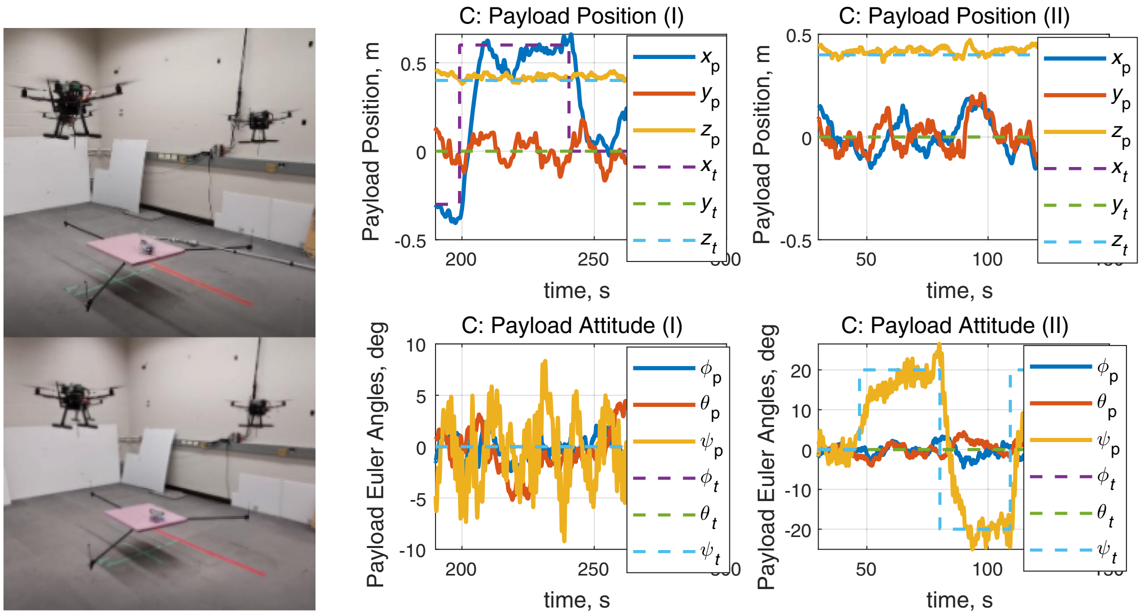

a)The disturbance rejection test **b) The position and attitude response of the payload**

Fig. A1 The disturbance rejection experiment.

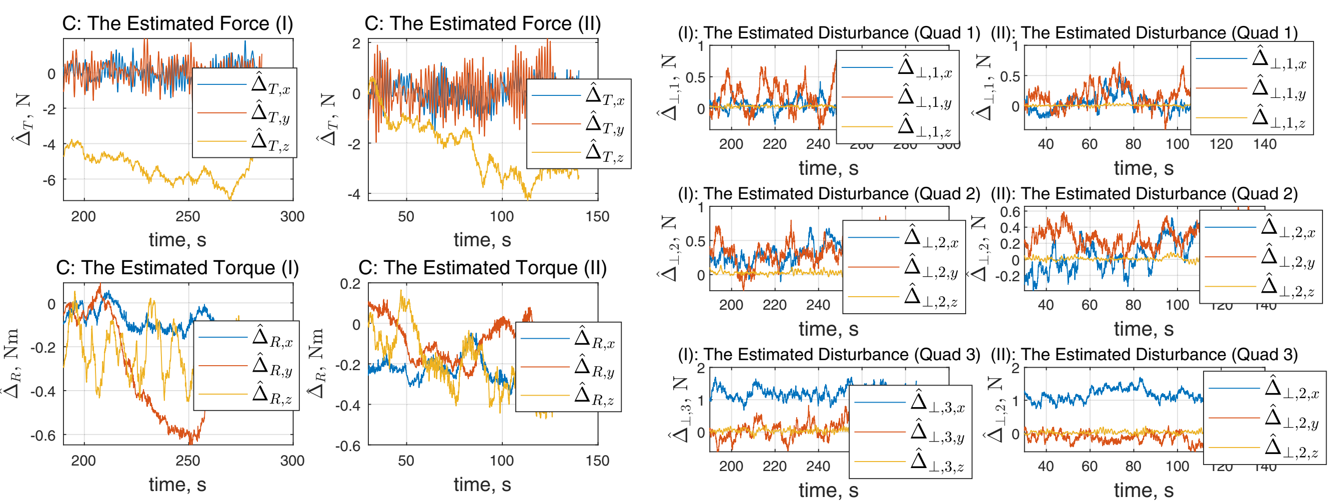

a) The estimated disturbances on the payload **b) The estimated disturbances on each quadrotor**

Fig. A2 The disturbance rejection experiment: estimated disturbances.

$\boldsymbol{M}\dot{\boldsymbol{u}}_d + \boldsymbol{C}\boldsymbol{u}_d$ terms are expanded as

$$
\begin{aligned}
&\boldsymbol{M}\dot{\boldsymbol{u}}_d + \boldsymbol{C}\boldsymbol{u}_d \\
&= \begin{bmatrix} m_p\dot{\boldsymbol{\xi}}^T \\ \boldsymbol{J}_p\boldsymbol{\eta} + \boldsymbol{\eta}^\times\boldsymbol{J}_p\boldsymbol{\omega}_p \\ \boldsymbol{0} \\ \vdots \\ \boldsymbol{0} \end{bmatrix} + \begin{bmatrix} \sum_{j=1}^N m_j(\boldsymbol{B}_j\dot{\boldsymbol{\mu}}_j + \dot{\boldsymbol{\xi}} - \boldsymbol{R}_{IP}\boldsymbol{t}_j^\times\dot{\boldsymbol{\eta}}) \\ \sum_{j=1}^N m_j\boldsymbol{t}_j^\times\boldsymbol{R}_{PI}(\boldsymbol{B}_j\dot{\boldsymbol{\mu}}_j + \dot{\boldsymbol{\xi}} - \boldsymbol{R}_{IP}\boldsymbol{t}_j^\times\dot{\boldsymbol{\eta}}) \\ \boldsymbol{B}_1^T m_1(\boldsymbol{B}_1\dot{\boldsymbol{\mu}}_1 + \dot{\boldsymbol{\xi}} - \boldsymbol{R}_{IP}\boldsymbol{t}_1^\times\dot{\boldsymbol{\eta}}) \\ \vdots \\ \boldsymbol{B}_N^T m_N(\boldsymbol{B}_N\dot{\boldsymbol{\mu}}_N + \dot{\boldsymbol{\xi}} - \boldsymbol{R}_{IP}\boldsymbol{t}_N^\times\dot{\boldsymbol{\eta}}) \end{bmatrix} \\
&+ \begin{bmatrix} \sum_{j=1}^N m_j(-\boldsymbol{R}_{IP}\boldsymbol{\omega}_p^\times\boldsymbol{t}_j^\times\boldsymbol{\eta} + \dot{\boldsymbol{B}}_j\boldsymbol{\mu}_j) \\ \sum_{j=1}^N \boldsymbol{t}_j^\times\boldsymbol{R}_{PI}m_j(-\boldsymbol{R}_{IP}\boldsymbol{\omega}_p^\times\boldsymbol{t}_j^\times\boldsymbol{\eta} + \dot{\boldsymbol{B}}_j\boldsymbol{\mu}_j) \\ \boldsymbol{B}_1^T m_1(-\boldsymbol{R}_{IP}\boldsymbol{\omega}_p^\times\boldsymbol{t}_1^\times\boldsymbol{\eta} + \dot{\boldsymbol{B}}_1\boldsymbol{\mu}_1) \\ \vdots \\ \boldsymbol{B}_N^T m_N(-\boldsymbol{R}_{IP}\boldsymbol{\omega}_p^\times\boldsymbol{t}_N^\times\boldsymbol{\eta} + \dot{\boldsymbol{B}}_N\boldsymbol{\mu}_N) \end{bmatrix}
\end{aligned} \tag{A5}
$$

Then $\boldsymbol{M}\dot{\boldsymbol{u}}_d + \boldsymbol{C}\boldsymbol{u}_d$ is expressed using the definition of $\boldsymbol{f}_{0,j}$ in Eq. (23) as

$$
\boldsymbol{M}\dot{\boldsymbol{u}}_d + \boldsymbol{C}\boldsymbol{u}_d = \begin{bmatrix} m_p\dot{\boldsymbol{\xi}} \\ \boldsymbol{J}_p\dot{\boldsymbol{\eta}} + \boldsymbol{\eta}^\times\boldsymbol{J}_p\boldsymbol{\omega}_p \\ \boldsymbol{0} \\ \vdots \\ \boldsymbol{0} \end{bmatrix} + \begin{bmatrix} -\sum_{j=1}^N \boldsymbol{f}_{0,j} \\ -\sum_{j=1}^N \boldsymbol{t}_j^\times\boldsymbol{R}_{PI}\boldsymbol{f}_{0,j} \\ -\boldsymbol{B}_1^T\boldsymbol{f}_{0,1} \\ \vdots \\ -\boldsymbol{B}_N^T\boldsymbol{f}_{0,N} \end{bmatrix} \tag{A6}
$$

The residues for the auxiliary terms caused by the estimation errors are

$$
\begin{cases} \tilde{\boldsymbol{\xi}} = \hat{\boldsymbol{\xi}} - \boldsymbol{\xi} = \tilde{\boldsymbol{F}}_1 \\ \tilde{\boldsymbol{\eta}} = \hat{\boldsymbol{\eta}} - \boldsymbol{\eta} = \tilde{\boldsymbol{F}}_2 \\ \tilde{\boldsymbol{\mu}} = \hat{\boldsymbol{\mu}} - \boldsymbol{\mu} = -k_L\tilde{\boldsymbol{r}}_{j,d} \end{cases}; \quad \begin{cases} \dot{\tilde{\boldsymbol{\xi}}} = -\lambda_1\tilde{\boldsymbol{F}}_1 + k_{r1}\tilde{\boldsymbol{R}}_1 \\ \dot{\tilde{\boldsymbol{\eta}}} = -\lambda_2\tilde{\boldsymbol{F}}_2 + k_{r2}\tilde{\boldsymbol{R}}_2 \end{cases} \tag{A7}
$$

$\hat{\boldsymbol{\Phi}}_j$ forms the $\boldsymbol{f}_{a,j}$ term in the virtual control force in Eq. (15), i.e., $\boldsymbol{f}_{a,j} = -K_0\hat{\boldsymbol{\Phi}}_j$. Based on the residue definition in Eq. (A7), the error between $\hat{\boldsymbol{f}}_{0,j}$ and $\boldsymbol{f}_{0,j}$ caused by the estimation error is defined as $\tilde{\boldsymbol{f}}_{0,j} = \hat{\boldsymbol{f}}_{0,j} - \boldsymbol{f}_{0,j}$:

$$\tilde{\boldsymbol{f}}_{0,j} = -m_j\Big[k_L\boldsymbol{B}_j\dot{\boldsymbol{r}}_{j,d} - \lambda_1\tilde{\boldsymbol{F}}_1 + k_{r1}\tilde{\boldsymbol{R}}_1 - \dot{\boldsymbol{B}}_j k_L\tilde{\boldsymbol{r}}_{j,d} - \boldsymbol{R}_{IP}\boldsymbol{\omega}_p^\times\boldsymbol{t}_j^\times\tilde{\boldsymbol{F}}_2 - \boldsymbol{R}_{IP}\boldsymbol{t}_j^\times\Big(-\lambda_2\tilde{\boldsymbol{F}}_2 + k_{r2}\tilde{\boldsymbol{R}}_2\Big)\Big] \tag{A8}$$

Combining the results from Eqs. (A1), (A4), (A6), and (A7), we have the following for $\dot{V}_1$:

$$\|\tilde{\boldsymbol{F}}_1\| \le \frac{k_{r1}}{\lambda_1}\|\tilde{\boldsymbol{R}}_1\|; \qquad \|\tilde{\boldsymbol{R}}_1\| \le \delta_r k_L\sum_{j=1}^N a_j\|\tilde{\boldsymbol{r}}_{j,d}\|;$$
$$\|\tilde{\boldsymbol{F}}_2\| \le \frac{k_{r2}}{\lambda_2}\|\tilde{\boldsymbol{R}}_2\|; \qquad \|\tilde{\boldsymbol{R}}_2\| \le \delta_r k_L\sum_{j=1}^N a_j\|\boldsymbol{E}_j^T\|\cdot\|\tilde{\boldsymbol{r}}_{j,d}\| \tag{A12}$$

We define vector $\boldsymbol{b}_j = \boldsymbol{\Delta}_T + \boldsymbol{R}_{IP}\boldsymbol{E}_j\boldsymbol{\Delta}_R$, $\hat{\boldsymbol{b}}_j = \hat{\boldsymbol{\Delta}}_T + \boldsymbol{R}_{IP}\boldsymbol{E}_j\hat{\boldsymbol{\Delta}}_R$, and vector $\tilde{\boldsymbol{b}}_j = \hat{\boldsymbol{b}}_j - \boldsymbol{b}_j$. Then we have the following inequality:

$$\dot{V}_1 = \begin{bmatrix} \boldsymbol{v}_p + \boldsymbol{\zeta} \\ \boldsymbol{\omega}_p + \boldsymbol{\eta} \\ \boldsymbol{v}_1 + \boldsymbol{\mu}_1 \\ \vdots \\ \boldsymbol{v}_N + \boldsymbol{\mu}_N \end{bmatrix}^T \left\{ \begin{bmatrix} m_p\dot{\boldsymbol{\zeta}} \\ \boldsymbol{J}_p\dot{\boldsymbol{\eta}} + \boldsymbol{\eta}^\times\boldsymbol{J}_p\boldsymbol{\omega}_p \\ \boldsymbol{0} \\ \vdots \\ \boldsymbol{0} \end{bmatrix} + \begin{bmatrix} \sum_{j=1}^N[-K_0\tilde{\boldsymbol{\Phi}}_j - a_j m_p\dot{\tilde{\boldsymbol{\zeta}}} - a_j\boldsymbol{R}_{IP}\boldsymbol{E}_j\boldsymbol{J}_p\dot{\tilde{\boldsymbol{\eta}}}] \\ \sum_{j=1}^N \boldsymbol{t}_j^\times\boldsymbol{R}_{PI}[-K_0\tilde{\boldsymbol{\Phi}}_j - a_j m_p\dot{\tilde{\boldsymbol{\zeta}}} - a_j\boldsymbol{R}_{IP}\boldsymbol{E}_j\boldsymbol{J}_p\dot{\tilde{\boldsymbol{\eta}}}] \\ \boldsymbol{B}_1^T[-K_0\tilde{\boldsymbol{\Phi}}_1 - a_1 m_p\dot{\tilde{\boldsymbol{\zeta}}} - a_1\boldsymbol{R}_{IP}\boldsymbol{E}_1\boldsymbol{J}_p\dot{\tilde{\boldsymbol{\eta}}}] \\ \vdots \\ \boldsymbol{B}_N^T[-K_0\tilde{\boldsymbol{\Phi}}_N - a_N m_p\dot{\tilde{\boldsymbol{\zeta}}} - a_N\boldsymbol{R}_{IP}\boldsymbol{E}_N\boldsymbol{J}_p\dot{\tilde{\boldsymbol{\eta}}}] \end{bmatrix} \right.$$
$$+ \begin{bmatrix} \sum_{j=1}^N[-K_0\boldsymbol{\Phi}_j - a_j(m_p\dot{\boldsymbol{\zeta}} + k_p m_p\boldsymbol{s}_p) - a_j\boldsymbol{R}_{IP}\boldsymbol{E}_j(\boldsymbol{J}_p\dot{\boldsymbol{\eta}} + k_\Omega\boldsymbol{s}_r)] \\ \sum_{j=1}^N \boldsymbol{t}_j^\times\boldsymbol{R}_{PI}[-K_0\boldsymbol{\Phi}_j - a_j(m_p\dot{\boldsymbol{\zeta}} + k_p m_p\boldsymbol{s}_p) - a_j\boldsymbol{R}_{IP}\boldsymbol{E}_j(\boldsymbol{J}_p\dot{\boldsymbol{\eta}}\eta + k_\Omega\boldsymbol{s}_r)] \\ \boldsymbol{B}_1^T[-K_0\boldsymbol{\Phi}_1 - a_1(m_p\dot{\boldsymbol{\zeta}} + k_p m_p\boldsymbol{s}_p) - a_1\boldsymbol{R}_{IP}\boldsymbol{E}_1(\boldsymbol{J}_p\dot{\boldsymbol{\eta}} + k_\Omega\boldsymbol{s}_r)] \\ \vdots \\ \boldsymbol{B}_N^T[-K_0\boldsymbol{\Phi}_N - a_N(m_p\dot{\boldsymbol{\zeta}} + k_p m_p\boldsymbol{s}_p) - a_N\boldsymbol{R}_{IP}\boldsymbol{E}_N(\boldsymbol{J}_p\dot{\boldsymbol{\eta}} + k_\Omega\boldsymbol{s}_r)] \end{bmatrix}$$
$$\left. + \begin{bmatrix} \sum_{j=1}^N(-\tilde{\boldsymbol{\Delta}}_{\perp,j} - a_j\tilde{\boldsymbol{\Delta}}_T - a_j\boldsymbol{R}_{IP}\boldsymbol{E}_j\tilde{\boldsymbol{\Delta}}_R + \tilde{\boldsymbol{f}}_{0,j}) \\ \sum_{j=1}^N \boldsymbol{t}_j^\times\boldsymbol{R}_{PI}(-\tilde{\boldsymbol{\Delta}}_{\perp,j} - a_j\tilde{\boldsymbol{\Delta}}_T - a_j\boldsymbol{R}_{IP}\boldsymbol{E}_j\tilde{\boldsymbol{\Delta}}_R + \tilde{\boldsymbol{f}}_{0,j}) \\ \boldsymbol{B}_1^T(-a_1(m_p\boldsymbol{g}_I + \boldsymbol{\Delta}_T + \boldsymbol{R}_{IP}\boldsymbol{E}_1\boldsymbol{\Delta}_R) - a_1\tilde{\boldsymbol{\Delta}}_T - a_1\boldsymbol{R}_{IP}\boldsymbol{E}_1\tilde{\boldsymbol{\Delta}}_R - \tilde{\boldsymbol{\Delta}}_{\perp,1} + \tilde{\boldsymbol{f}}_{0,1}) \\ \vdots \\ \boldsymbol{B}_N^T(-a_N(m_p\boldsymbol{g}_I + \boldsymbol{\Delta}_T + \boldsymbol{R}_{IP}\boldsymbol{E}_N\boldsymbol{\Delta}_R) - a_N\tilde{\boldsymbol{\Delta}}_T - a_N\boldsymbol{R}_{IP}\boldsymbol{E}_N\tilde{\boldsymbol{\Delta}}_R - \tilde{\boldsymbol{\Delta}}_{\perp,N} + \tilde{\boldsymbol{f}}_{0,N}) \end{bmatrix} \right\} \tag{A9}$$

where $\boldsymbol{h}_j$ denotes the effect of $-K_0\tilde{\boldsymbol{\Phi}}_j - a_j m_p\dot{\tilde{\boldsymbol{\zeta}}} - a_j\boldsymbol{R}_{IP}\boldsymbol{E}_j\boldsymbol{J}_p\dot{\tilde{\boldsymbol{\eta}}} - \tilde{\boldsymbol{\Delta}}_{\perp,j} - a_j\tilde{\boldsymbol{\Delta}}_T - a_j\boldsymbol{R}_{IP}\boldsymbol{E}_j\tilde{\boldsymbol{\Delta}}_R + \tilde{\boldsymbol{f}}_{0,j}$ caused by the disturbance estimation errors $\tilde{\boldsymbol{\Delta}}_T$ and $\tilde{\boldsymbol{\Delta}}_R$. It is expanded as follows:

$$\boldsymbol{h}_j = m_j k_L\dot{\boldsymbol{B}}\tilde{\boldsymbol{r}}_{j,d} + K_0 k_L\boldsymbol{B}_j\tilde{\boldsymbol{r}}_{j,d} + (m_j\lambda_1 - K_0 + a_j m_p\lambda_1)\tilde{\boldsymbol{F}}_1 - (m_j + a_j m_p)k_{r1}\tilde{\boldsymbol{R}}_1 + \boldsymbol{R}_{IP}\Big(m_j\boldsymbol{\omega}_p^\times\boldsymbol{t}_j^\times - m_j\lambda_2\boldsymbol{t}_j^\times + K_0\boldsymbol{t}_j^\times + a_j\lambda_2\boldsymbol{E}_j\boldsymbol{J}_p\Big)\tilde{\boldsymbol{F}}_2 + \boldsymbol{R}_{IP}\Big(m_j\boldsymbol{t}_j^\times - a_j\boldsymbol{E}_j\boldsymbol{J}_p\Big)k_{r2}\tilde{\boldsymbol{R}}_2 \tag{A10}$$

Now we analyze the detailed structure of $\boldsymbol{h}_j$. Based on Eq. (14), $\boldsymbol{F}_1$ and $\boldsymbol{F}_2$ can be viewed as passing $\boldsymbol{R}_1$ and $\boldsymbol{R}_2$ through first-order systems, so $\tilde{\boldsymbol{F}}_1$ and $\tilde{\boldsymbol{F}}_2$ can be expressed in the frequency domain as

$$\tilde{F}_1(s) = k_{r1}\tilde{\boldsymbol{R}}_1/(s+\lambda_1); \quad \tilde{\boldsymbol{F}}_2(s) = k_{r2}\tilde{\boldsymbol{R}}_2/(s+\lambda_2) \tag{A11}$$

If the initial condition of $\boldsymbol{F}_1$, $\boldsymbol{F}_2$, $\hat{\boldsymbol{F}}_1$, and $\hat{\boldsymbol{F}}_2$ are set to $\boldsymbol{0}$ for simplification, according to Lemma 1 (ii), the bounds of $\hat{\boldsymbol{F}}_1$, $\tilde{\boldsymbol{F}}_2$, $\tilde{\boldsymbol{R}}_1$, and $\tilde{\boldsymbol{R}}_2$ can be related to $\tilde{\boldsymbol{r}}_{j,d}$ as

$$\tilde{\boldsymbol{r}}_{j,d}/l = \frac{\hat{\boldsymbol{b}}_{j,xy}}{\|m_p\boldsymbol{g}_I + \hat{\boldsymbol{b}}_j\|} - \frac{\boldsymbol{b}_{j,xy}}{\|m_p\boldsymbol{g}_I + \boldsymbol{b}_j\|} = \left[\tilde{\boldsymbol{b}}_{j,xy} + \boldsymbol{b}_{j,xy}\left(1 - \frac{\|m_p\boldsymbol{g}_I + \hat{\boldsymbol{b}}_j\|}{\|m_p\boldsymbol{g}_I + \boldsymbol{b}_j\|}\right)\right]\Big/\|m_p\boldsymbol{g}_I + \hat{\boldsymbol{b}}_j\| \tag{A13}$$

Hence the magnitude of $\tilde{\boldsymbol{r}}_{j,d}/l$ satisfies the following:

$$\begin{aligned}\|\tilde{\boldsymbol{r}}_{j,d}\|/l &\le \frac{\|\tilde{\boldsymbol{b}}_j\|\cdot\|m_p\boldsymbol{g}_I + \boldsymbol{b}_j\| + \|\boldsymbol{b}_{j,xy}\|\cdot\|m_p\boldsymbol{g}_I + \hat{\boldsymbol{b}}_j - m_p\boldsymbol{g}_I - \boldsymbol{b}_j\|}{\|m_p\boldsymbol{g}_I + \boldsymbol{b}_j\|\cdot\|m_p\boldsymbol{g}_I + \hat{\boldsymbol{b}}_j\|} \\ &= \frac{\|\tilde{\boldsymbol{b}}_j\|\cdot\|m_p\boldsymbol{g}_I + \boldsymbol{b}_j\| + \|\boldsymbol{b}_{j,xy}\|\cdot\|\tilde{\boldsymbol{b}}_j\|}{\|m_p\boldsymbol{g}_I + \boldsymbol{b}_j\|\cdot\|m_p\boldsymbol{g}_I + \hat{\boldsymbol{b}}_j\|} \\ &= \frac{\|m_p\boldsymbol{g}_I + \boldsymbol{b}_j\| + \|\boldsymbol{b}_{j,xy}\|}{\|m_p\boldsymbol{g}_I + \boldsymbol{b}_j\|\cdot\|m_p\boldsymbol{g}_I + \hat{\boldsymbol{b}}_j\|}\|\tilde{\boldsymbol{b}}_j\| \\ &\le \frac{\|m_p\boldsymbol{g}_I + \boldsymbol{b}_j\| + \|\boldsymbol{b}_{j,xy}\|}{\|m_p\boldsymbol{g}_I + \boldsymbol{b}_j\|\cdot\|m_p\boldsymbol{g}_I + \hat{\boldsymbol{b}}_j\|}\Big(\|\tilde{\boldsymbol{\Delta}}_T\| + \|\boldsymbol{E}_j\tilde{\boldsymbol{\Delta}}_R\|\Big)\end{aligned} \tag{A14}$$

To sum up, $\tilde{\boldsymbol{r}}_{j,d}$ can be related to the disturbance estimation errors as

$$\|\tilde{\boldsymbol{r}}_{j,d}\|/l \le \beta_j(\|\tilde{\boldsymbol{\Delta}}_T\| + \|\boldsymbol{E}_j\| \cdot \|\tilde{\boldsymbol{\Delta}}_R\|);$$
$$\beta_j = \frac{\|m_p\boldsymbol{g}_I + \boldsymbol{b}_j\| + \|\boldsymbol{b}_{j,xy}\|}{\|m_p\boldsymbol{g}_I + \boldsymbol{b}_j\| \cdot \|m_p\boldsymbol{g}_I + \hat{\boldsymbol{b}}_j\|} \tag{A15}$$

As a result, the bound of $\tilde{\boldsymbol{R}}_1$ and $\tilde{\boldsymbol{R}}_2$ based on the disturbance estimation errors are

$$\|\tilde{\boldsymbol{R}}_1\| \le \delta_r k_L \sum_{j=1}^{N} a_j l\beta_j\Big(\|\tilde{\boldsymbol{\Delta}}_T\| + \|\boldsymbol{E}_j\| \cdot \|\tilde{\boldsymbol{\Delta}}_R\|\Big)$$
$$\le \left(\delta_r k_L \sum_{j=1}^{N} a_j l\beta_j\right)\|\tilde{\boldsymbol{\Delta}}_T\| + \left(\delta_r k_L \sum_{j=1}^{N} a_j l\beta_j\right)E_0\|\tilde{\boldsymbol{\Delta}}_R\| \tag{A16}$$

$$\|\tilde{\boldsymbol{R}}_2\| \le \delta_r k_L \sum_{j=1}^{N} l\beta_j a_j\|\boldsymbol{E}_j\|\Big(\|\tilde{\boldsymbol{\Delta}}_T\| + \|\boldsymbol{E}_j\| \cdot \|\tilde{\boldsymbol{\Delta}}_R\|\Big)$$
$$\le \left(\delta_r k_L \sum_{j=1}^{N} l\beta_j a_j\|\boldsymbol{E}_j\|\right)\|\tilde{\boldsymbol{\Delta}}_T\|$$
$$+ \left(\delta_r k_L \sum_{j=1}^{N} l\beta_j a_j\|\boldsymbol{E}_j\|\right)E_0\|\tilde{\boldsymbol{\Delta}}_R\| \tag{A17}$$

where E_0 is defined in Eq. (21). Hence, by expanding Eq. (A10), the relationship among $\boldsymbol{h}_j$, $\tilde{\boldsymbol{\Delta}}_T$, and $\tilde{\boldsymbol{\Delta}}_R$ is summarized as follows:

$$\|\boldsymbol{h}_j\| \le h_{\delta,j}\|\tilde{\boldsymbol{\Delta}}_T\| + E_0 h_{\delta,j}\|\tilde{\boldsymbol{\Delta}}_R\|;$$
$$h_{\delta,j} = lk_L\delta_r(k_{r1}(\epsilon_1+\epsilon_2)\alpha_1 + k_{r2}(\epsilon_3+\epsilon_4)\alpha_2 + \beta_j(K_0 + m_j\delta_r\delta_v))$$
$$\alpha_1 = \sum_{j=1}^{N} a_j\beta_j;\ \ \alpha_2 = \sum_{j=1}^{N} a_j\beta_j\|\boldsymbol{E}_j^T\|;$$
$$\epsilon_1 = |m_j\lambda_1 - K_0 + a_j m_p\lambda_1|/\lambda_1;\quad \epsilon_2 = m_j + a_j m_p;$$
$$\epsilon_3 = \Big(\|m_j\lambda_2 t_j^{\times} - K_0 t_j^{\times} - a_j\lambda_2\boldsymbol{E}_j\boldsymbol{J}_p\| + m_j\|\boldsymbol{t}_j\|\delta_\omega\Big)/\lambda_2;$$
$$\epsilon_4 = \big\|m_j\boldsymbol{t}_j^{\times} - a_j\boldsymbol{E}_j\boldsymbol{J}_p\big\| \tag{A18}$$

$h_{\delta,j}$ is bounded as explained in Remark 2 by using the result of $\dot{V}_4$. This property is later used in Remark 3 to conclude the stability of the entire system. Note that $\boldsymbol{f}_{d,j}/\|\boldsymbol{f}_{d,j}\| = \boldsymbol{L}_{j,d}/l$. According to Lemma 1 (iii), we have the following inequality:

$$\boldsymbol{\mu}_j^T\boldsymbol{B}_j^T\boldsymbol{f}_{d,j}/\|\boldsymbol{f}_{d,j}\| = \boldsymbol{\mu}_j^T\boldsymbol{B}_j^T\boldsymbol{L}_{j,d}/l$$
$$= k_L\left(\tilde{\boldsymbol{r}}_j^T\boldsymbol{r}_{j,d} - \tilde{\boldsymbol{r}}_j^T\boldsymbol{r}_j\sqrt{l^2 - \boldsymbol{r}_{j,d}^2}/\sqrt{l^2 - \boldsymbol{r}_j^2}\right)/l$$
$$= \frac{k_L\left(-\tilde{\boldsymbol{r}}_j^2\sqrt{l^2 - \boldsymbol{r}_{j,d}^2} + \tilde{\boldsymbol{r}}_j^T\boldsymbol{r}_{j,d}\left(\sqrt{l^2 - \boldsymbol{r}_j^2} - \sqrt{l^2 - \boldsymbol{r}_{j,d}^2}\right)\right)}{l\sqrt{l^2 - \boldsymbol{r}_j^2}}$$
$$\le \frac{k_L(-\cos\theta_d + C_r\sin\theta_d)\tilde{\boldsymbol{r}}_j^2}{\sqrt{l^2 - \boldsymbol{r}_j^2}} \tag{A19}$$

The above inequality is feasible when $\|\boldsymbol{r}_{j,d}\|/l$ is within a certain bound; i.e., the effective disturbances are bounded and small compared with the weight of the payload. Some of the error terms in Eq. (A9) become

$$\begin{bmatrix} \boldsymbol{v}_p+\boldsymbol{\zeta} \\ \boldsymbol{\omega}_p+\boldsymbol{\eta} \\ \boldsymbol{v}_1+\boldsymbol{\mu}_1 \\ \vdots \\ \boldsymbol{v}_N+\boldsymbol{\mu}_N \end{bmatrix}^T \begin{bmatrix} -k_p m_p\boldsymbol{s}_p \\ \boldsymbol{\eta}^{\times}\boldsymbol{J}_p\boldsymbol{\omega}_p - k_\Omega\boldsymbol{s}_r \\ \boldsymbol{B}_1^T\big[-a_1(m_p\dot{\boldsymbol{\zeta}} + k_p m_p\boldsymbol{s}_p) - a_1\boldsymbol{R}_{IP}\boldsymbol{E}_1(\boldsymbol{J}_p\dot{\boldsymbol{\eta}} + k_\Omega\boldsymbol{s}_r)\big] \\ \vdots \\ \boldsymbol{B}_N^T\big[-a_N(m_p\dot{\boldsymbol{\zeta}} + k_p m_p\boldsymbol{s}_p) - a_N\boldsymbol{R}_{IP}\boldsymbol{E}_N(\boldsymbol{J}_p\dot{\boldsymbol{\eta}} + k_\Omega\boldsymbol{s}_r)\big] \end{bmatrix}$$
$$= -k_p m_p\boldsymbol{s}_p^2 - k_p m_p\boldsymbol{F}_1^T\boldsymbol{s}_p - \boldsymbol{\eta}^T\boldsymbol{\omega}_p^{\times}\boldsymbol{J}_p\boldsymbol{\omega} - k_\Omega\boldsymbol{s}_r^2 - k_\Omega\boldsymbol{F}_2^T\boldsymbol{s}_r$$
$$-m_p\boldsymbol{R}_1^T\Big(k_v\dot{\boldsymbol{e}}_{p_i} - \lambda_1\boldsymbol{F}_1 + k_{r1}\boldsymbol{R}_1\Big) - m_p k_p\boldsymbol{R}_1^T\boldsymbol{s}_p$$
$$-\boldsymbol{R}_2^T\boldsymbol{J}_p\Big(k_r\dot{\boldsymbol{e}}_r - \lambda_2\boldsymbol{F}_2 + k_{r2}\boldsymbol{R}_2\Big) - k_\Omega\boldsymbol{R}_2^T\boldsymbol{s}_r \tag{A20}$$

Finally, according to $G_{r,j}$ and $\boldsymbol{f}_{d,j}$ defined in Eqs. (21) and (23), we combine Eqs. (A9), (A18), (A19), and (A20) to obtain $\dot{V}_1$.

Appendix B: Proof of Proposition 2

Now we proceed to calculate the time derivative of $V_{2,j}$. We firstly provide several derivative properties for $\boldsymbol{L}_{j,d}$. Since the length of $\boldsymbol{L}_{j,d}$ is fixed as l, we have the following relationship:

$$2\boldsymbol{L}_{j,d}^T\dot{\boldsymbol{L}}_{j,d} = \frac{d}{dt}(\boldsymbol{L}_{j,d}^T\boldsymbol{L}_{j,d}) = \frac{dl^2}{dt} = 0;$$
$$\boldsymbol{f}_{d,j}^T\dot{\boldsymbol{L}}_{j,d} = \|\boldsymbol{f}_{d,j}\|\boldsymbol{L}_{j,d}^T\dot{\boldsymbol{L}}_{j,d}/l = 0 \tag{B1}$$

Since $\dot{\boldsymbol{f}}_{d,j} = -a_j\boldsymbol{R}_{IP}\boldsymbol{\omega}_p^{\times}\boldsymbol{E}_j\boldsymbol{\Delta}_R$, we have the following inequality property:

$$\|\dot{\boldsymbol{f}}_{d,j}\| \le a_j\|\boldsymbol{\omega}_p\| \cdot \|\boldsymbol{E}_j\boldsymbol{\Delta}_R\| \tag{B2}$$

Since $\boldsymbol{f}_{d,j}^T\boldsymbol{f}_{d,j} = \|\boldsymbol{f}_{d,j}\|^2$, we have the following:

$$\frac{d}{dt}(\|\boldsymbol{f}_{d,j}\|) = \frac{\boldsymbol{f}_{d,j}^T\dot{\boldsymbol{f}}_{d,j}}{\|\boldsymbol{f}_{d,j}\|} \tag{B3}$$

The cable vector $\boldsymbol{L}_{j,d}$ varies with time before the system settles, so its time derivative is

$$\dot{\boldsymbol{L}}_{j,d} = l\frac{d}{dt}\frac{\boldsymbol{f}_{d,j}}{\|\boldsymbol{f}_{d,j}\|} = l\frac{\dot{\boldsymbol{f}}_{j,d}\|\boldsymbol{f}_{d,j}\| - \boldsymbol{f}_{j,d}\boldsymbol{f}_{j,d}^T\dot{\boldsymbol{f}}_{j,d}/\|\boldsymbol{f}_{d,j}\|}{\|\boldsymbol{f}_{d,j}\|^2}$$
$$= -l\Big(\boldsymbol{1} - \boldsymbol{f}_{j,d}\boldsymbol{f}_{j,d}^T/\|\boldsymbol{f}_{d,j}\|^2\Big)a_j\boldsymbol{R}_{IP}\boldsymbol{\omega}_p^{\times}\boldsymbol{E}_j\boldsymbol{\Delta}_R/\|\boldsymbol{f}_{d,j}\| \tag{B4}$$

The above equation means that the norm of $\dot{\boldsymbol{L}}_{j,d}$ and $\dot{\boldsymbol{r}}_{j,d}$ are bounded by the angular velocity of the payload:

$$\|\dot{\boldsymbol{L}}_{j,d}\| \le l\|\boldsymbol{\omega}_p\|\delta_R;\quad \|\dot{\boldsymbol{r}}_{j,d}\| \le \|\dot{\boldsymbol{L}}_{j,d}\| \le l\|\boldsymbol{\omega}_p\|\delta_R \tag{B5}$$

where δ_R defined in Eq. (21). The time derivative of $\|\boldsymbol{f}_{d,j}\|(l - \boldsymbol{L}_{j,d}^T\boldsymbol{L}_j/l)/a_j$ is as follows:

$$\frac{d}{dt}(\|\boldsymbol{f}_{d,j}\|(l - \boldsymbol{L}_{j,d}^T\boldsymbol{L}_j/l)) = \dot{\boldsymbol{f}}_{d,j}^T(\boldsymbol{L}_{j,d} - \boldsymbol{L}_j) + \boldsymbol{f}_{d,j}^T(\dot{\boldsymbol{L}}_{j,d} - \dot{\boldsymbol{L}}_j)$$
$$= -\|\boldsymbol{f}_{d,j}\|\boldsymbol{L}_{j,d}^T\boldsymbol{B}_j\boldsymbol{v}_j/l + \dot{\boldsymbol{f}}_{d,j}^T(\boldsymbol{L}_{j,d} - \boldsymbol{L}_j);$$
$$\frac{d}{dt}(m_p\Xi_1\tilde{\boldsymbol{L}}_j^T\boldsymbol{F}_1) = -m_p\Xi_1\Big[(\boldsymbol{B}_j(\boldsymbol{v}_j + \boldsymbol{\mu}_j))^T - (\boldsymbol{B}_j\boldsymbol{\mu}_j)^T$$
$$- \dot{\boldsymbol{L}}_{j,d}^T\Big]\boldsymbol{F}_1 - \Xi_1\lambda_1 m_p\tilde{\boldsymbol{L}}_j^T\boldsymbol{F}_1$$
$$+ \Xi_1 m_p k_{r1}\tilde{\boldsymbol{L}}_j^T\boldsymbol{R}_1 \tag{B6}$$

$$
\begin{aligned}
&\frac{d}{dt}\left(\Xi_2 \tilde{\boldsymbol{L}}_j^T \boldsymbol{R}_{IP} \boldsymbol{E}_j \boldsymbol{J}_p \boldsymbol{F}_2\right)\\
&\quad= \Xi_2\Big[\Big(\dot{\boldsymbol{L}}_{j,d} - \boldsymbol{B}_j(\boldsymbol{v}_j+\boldsymbol{\mu}_j) + \boldsymbol{B}_j\boldsymbol{\mu}_j\Big)^T \boldsymbol{R}_{IP}\boldsymbol{E}_j\boldsymbol{J}_p\boldsymbol{F}_2\\
&\qquad + \tilde{\boldsymbol{L}}_j^T \boldsymbol{R}_{IP}\boldsymbol{\omega}_p^\times \boldsymbol{E}_j \boldsymbol{J}_p \boldsymbol{F}_2 + k_{r2}\tilde{\boldsymbol{L}}_j^T \boldsymbol{R}_{IP}\boldsymbol{E}_j\boldsymbol{J}_p\boldsymbol{R}_2 - \lambda_2 \tilde{\boldsymbol{L}}_j^T \boldsymbol{R}_{IP} \boldsymbol{E}_j \boldsymbol{J}_p \boldsymbol{F}_2\Big]
\end{aligned}
\tag{B7}
$$

The derivatives of the quadratic terms are

$$
\begin{aligned}
&\frac{1}{2}\frac{d}{dt}(m_p k_{F1}\boldsymbol{F}_1^T\boldsymbol{F}_1) = -m_p\lambda_1 k_{F1}\boldsymbol{F}_1^2 + m_p k_{F1}k_{r1}\boldsymbol{F}_1^T\boldsymbol{R}_1;\\
&\frac{1}{2}\frac{d}{dt}(k_{F2}\boldsymbol{F}_2^T\boldsymbol{J}_p\boldsymbol{F}_2) = -k_{F2}\lambda_2\boldsymbol{\mathcal{F}}_2^2 + k_{F2}k_{r2}\boldsymbol{\mathcal{F}}_2^T\mathcal{R}_2
\end{aligned}
\tag{B8}
$$

According to Lemma 1 (i) and (ii), we have the time derivative of $V_{2,j}$ by summing up all the subterms above as

$$
\begin{aligned}
L_f V_{2,j} = &-\|\boldsymbol{f}_{d,j}\|\boldsymbol{L}_{j,d}^T\boldsymbol{B}_j\boldsymbol{v}_j/(la_j) + \gamma_j\|\boldsymbol{E}_j\boldsymbol{\Delta}_R\|\cdot\|\boldsymbol{\omega}_p\|\cdot\|\tilde{\boldsymbol{r}}_j\|\\
&+ \Xi_1 m_p\Big[-(\boldsymbol{B}_j(\boldsymbol{v}_j+\boldsymbol{\mu}_j))^T\boldsymbol{F}_1 + (\boldsymbol{B}_j\boldsymbol{\mu}_j)^T\boldsymbol{F}_1\\
&+ \tilde{\boldsymbol{L}}_j^T(-\lambda_1\boldsymbol{F}_1 + k_{r1}\boldsymbol{R}_1) + \dot{\boldsymbol{L}}_{j,d}^T\boldsymbol{F}_1\Big] - m_p\lambda_1 k_{F1}\boldsymbol{F}_1^2\\
&+ m_p k_{F1}k_{r1}\boldsymbol{F}_1^T\boldsymbol{R}_1 + \Xi_2\Big[-(\boldsymbol{B}_j(\boldsymbol{v}_j+\boldsymbol{\mu}_j))^T\boldsymbol{R}_{IP}\boldsymbol{E}_j\boldsymbol{J}_p\boldsymbol{F}_2\\
&+ (\boldsymbol{B}_j\boldsymbol{\mu}_j)^T\boldsymbol{R}_{IP}\boldsymbol{E}_j\boldsymbol{J}_p\boldsymbol{F}_2 + \dot{\boldsymbol{L}}_{j,d}^T\boldsymbol{R}_{IP}\boldsymbol{E}_j\boldsymbol{J}_p\boldsymbol{F}_2\\
&+ \tilde{\boldsymbol{L}}_j^T\boldsymbol{R}_{IP}\boldsymbol{\omega}_p^\times\boldsymbol{E}_j\boldsymbol{J}_p\boldsymbol{F}_2 + \tilde{\boldsymbol{L}}_j^T\boldsymbol{R}_{IP}\boldsymbol{E}_j(k_{r2}\boldsymbol{J}_p\boldsymbol{R}_2 - \lambda_2\boldsymbol{J}_p\boldsymbol{F}_2)\Big]\\
&- k_{F2}\lambda_2\boldsymbol{\mathcal{F}}_2^2 + k_{F2}k_{r2}\boldsymbol{\mathcal{F}}_2^T\mathcal{R}_2
\end{aligned}
\tag{B9}
$$

According to Lemma 1 (i) and (ii), the following inequalities are true:

$$
\begin{aligned}
(\boldsymbol{B}_j\boldsymbol{\mu}_j)^T\boldsymbol{F}_1 &\le k_L\delta_r\|\tilde{\boldsymbol{r}}_j\|\cdot\|\boldsymbol{F}_1\|;\\
(\boldsymbol{B}_j\boldsymbol{\mu}_j)^T\boldsymbol{R}_{IP}\boldsymbol{E}_j\boldsymbol{J}_p\boldsymbol{F}_2 &\le k_L\delta_r\sigma_j\|\tilde{\boldsymbol{r}}_j\|\cdot\|\boldsymbol{\mathcal{F}}_2\|
\end{aligned}
\tag{B10}
$$

Based on the definitions of Ξ_1 and Ξ_2 in Eq. (21), we have the following identity:

$$
\begin{aligned}
&m_p\Xi_1\sum_{j=1}^N a_j\Big[-(\boldsymbol{B}_j(\boldsymbol{v}_j+\boldsymbol{\mu}_j))^T\Big]\boldsymbol{F}_1 + m_p k_{r1}k_{F1}\boldsymbol{F}_1^T\boldsymbol{R}_1\\
&\quad= -m_p\lambda_1\boldsymbol{R}_1^T\boldsymbol{F}_1,\\
&\Xi_2\sum_{j=1}^N a_j\Big[-(\boldsymbol{B}_j(\boldsymbol{v}_j+\boldsymbol{\mu}_j))^T\boldsymbol{R}_{IP}\boldsymbol{E}_j\Big]\boldsymbol{J}_p\boldsymbol{F}_2 + k_{F2}k_{r2}\boldsymbol{\mathcal{F}}_2^T\mathcal{R}_2\\
&\quad= -\lambda_2\boldsymbol{\mathcal{F}}_2^T\mathcal{R}_2
\end{aligned}
\tag{B11}
$$

Combining Eqs. (B9), (B10), and (B11), we can obtain the conclusion of Proposition 2.

Appendix C: Proof of Proposition 3

$$
\begin{aligned}
\dot V_4 =& c_T\tilde{\boldsymbol{\Delta}}_T^T\dot{\tilde{\boldsymbol{\Delta}}}_T + c_R\tilde{\boldsymbol{\Delta}}_R^T\dot{\tilde{\boldsymbol{\Delta}}}_R\\
&+\sum_{j=1}^N\Big[(a_jc_R\lambda_R N^2\Gamma_c^2 + c_T\lambda_T N)/(2\kappa_j) + c_ja_j\Big]\tilde{\boldsymbol{\Delta}}_j^T\dot{\tilde{\boldsymbol{\Delta}}}_j\\
=& -\lambda_T c_T\tilde{\boldsymbol{\Delta}}_T^T\Big(\tilde{\boldsymbol{\Delta}}_T + \sum_{j=1}^N\tilde{\boldsymbol{\Delta}}_{\perp,j}\Big) - \lambda_R c_R\tilde{\boldsymbol{\Delta}}_R^T\Big(\tilde{\boldsymbol{\Delta}}_R + \sum_{i=1}^N\boldsymbol{t}_i^\times\boldsymbol{R}_{PI}\tilde{\boldsymbol{\Delta}}_{\perp,i}\Big)\\
&-\sum_{j=1}^N\Big[(a_jc_R\lambda_R N^2\Gamma_c^2 + c_T\lambda_T N)/2 + c_ja_j\kappa_j\Big]\tilde{\boldsymbol{\Delta}}_j^T\mathfrak{B}_j\tilde{\boldsymbol{\Delta}}_j\\
\le& -\sum_{j=1}^N a_j\Big[\frac{1}{2}\lambda_T c_T\tilde{\boldsymbol{\Delta}}_T^2 + \frac{1}{2}\lambda_R c_R\tilde{\boldsymbol{\Delta}}_R^2 + c_j\kappa_j\tilde{\boldsymbol{\Delta}}_{\perp,j}^2\Big]\\
&-\sum_{j=1}^N\Big[\frac{\lambda_T c_T}{2N}\tilde{\boldsymbol{\Delta}}_T^2 - c_T\lambda_T\|\tilde{\boldsymbol{\Delta}}_T\|\cdot\|\tilde{\boldsymbol{\Delta}}_{\perp,j}\| + \frac{c_T\lambda_T N}{2}\tilde{\boldsymbol{\Delta}}_{\perp,j}^2\Big]\\
&-\sum_{j=1}^N\sum_{i=1}^N\Big[\frac{\lambda_R c_R a_j}{2N}\tilde{\boldsymbol{\Delta}}_R^2 - a_j\lambda_R c_R\Gamma_c\|\tilde{\boldsymbol{\Delta}}_R\|\cdot\|\tilde{\boldsymbol{\Delta}}_{\perp,i}\| + \frac{a_jc_R\lambda_R\Gamma_c^2 N}{2}\tilde{\boldsymbol{\Delta}}_{\perp,i}^2\Big]\\
\le& -\sum_{j=1}^N a_j\Big[\frac{1}{2}\lambda_T c_T\tilde{\boldsymbol{\Delta}}_T^2 + \frac{1}{2}\lambda_R c_R\tilde{\boldsymbol{\Delta}}_R^2 + c_j\kappa_j\tilde{\boldsymbol{\Delta}}_{\perp,j}^2\Big]\le 0
\end{aligned}
\tag{C1}
$$

Acknowledgments

This research was sponsored by Natural Science and Engineering Council of Canada (NSERC) Collaborative Research and Training Experience Program (CREATE) (Funding No. 466088), NSERC Collaborative Research Program in collaboration with Drone Delivery Canada (Funding No. CRDPJ 508381-16), and Ontario Trillium Scholarship (OTS).

References

[1] Scaramuzza, D., Achtelik, M. C., Doitsidis, L., Friedrich, F., Kosmatopoulos, E., Martinelli, A., Achtelik, M. W., Chli, M., Chatzichristofis, S., and Kneip, L., "Vision-Controlled Micro Flying Robots: From System Design to Autonomous Navigation and Mapping in GPS-Denied Environments," *IEEE Robotics and Automation Magazine*, Vol. 21, No. 3, 2014, pp. 26–40.

[2] Merino, L., Caballero, F., de Dios, M., Jr., Maza, I., and Ollero, A., "An Unmanned Aircraft System for Automatic Forest Fire Monitoring and Measurement," *Journal of Intelligent and Robotic Systems*, Vol. 65, No. 1, 2012, pp. 533–548.

[3] Bernard, M., and Kondak, K., "Generic Slung Load Transportation System Using Small Size Helicopters," *IEEE International Conference on Robotics and Automation, ICRA'09*, Inst. of Electrical and Electronics Engineers, New York, 2009, pp. 3258–3264.
https://doi.org/10.1109/AERO.2017.7943815

[4] Maza, I., Kondak, K., Bernard, M., and Ollero, A., "Multi-UAV Cooperation and Control for Load Transportation and Deployment," *Journal of Intelligent and Robotic Systems*, Vol. 57, Nos. 1–4, 2010, pp. 417–449.
https://doi.org/10.1007/s10846-009-9352-8

[5] Ivler, C., Tischler, M., and Powell, J. D., "Cable Angle Feedback Control Systems to Improve Handling Qualities for Helicopters with Slung Loads," *AIAA Guidance, Navigation, and Control Conference*, AIAA Paper 2011-6686, 2011.
https://doi.org/10.2514/6.2011-6686

[6] Qian, L., and Liu, H. H. T., "Path Following Control of a Quadrotor UAV with a Cable Suspended Payload Under Wind Disturbances," *IEEE Transactions on Industrial Electronics*, Vol. 67, No. 3, 2019, pp. 2021–2029.

[7] McGonagle, J. G., "The Design, Test, and Development Challenges of Converting the K-MAX Helicopter to a Heavy Lift Rotary Wing UAV," *57th AHS International Annual Forum*, American Helicopter Soc. (AHS) International, Washington, D.C., 2001, pp. 1–11.

[8] Klausen, K., Meissen, C., Fossen, T. I., Arcak, M., and Johansen, T. A., "Cooperative Control for Multirotors Transporting an Unknown Suspended Load Under Environmental Disturbances," *IEEE Transactions*

on Control Systems Technology, Vol. 28, No. 2, 2020, pp. 653–660. https://doi.org/10.1109/TCST.2018.2876518

[9] Geng, J., and Langelaan, J. W., "Cooperative Transport of a Slung Load Using Load-Leading Control," *Journal of Guidance, Control, and Dynamics*, Vol. 43, No. 7, 2020, pp. 1313–1331.

[10] Smirnov, G., "Multiple-Power-Path Nonplanetary Main Gearbox of the Mi-26 Heavy-Lift Transport Helicopter," *Vertiflite*, Vol. 36, 1990, pp. 20–23.

[11] Duffy, M., and Samaritano, T., "The Lift! Project–Modular, Electric Vertical Lift System," *33rd AIAA Applied Aerodynamics Conference*, Vol. 71, AIAA, Reston, VA, June 2015, pp. 1–20. https://doi.org/10.2514/6.2015-3013

[12] Qian, L., and Liu, H. H., "Path Following Control of Multiple Quadrotors Carrying a Rigid-Body Slung Payload," *AIAA Scitech 2019 Forum*, AIAA Paper 2019-1172, 2019. https://doi.org/10.2514/6.2019-1172

[13] Lee, T., "Geometric Control of Multiple Quadrotor UAVs Transporting a Cable-Suspended Rigid Body," *2014 IEEE 53rd Annual Conference on Decision and Control (CDC)*, Inst. of Electrical and Electronics Engineers, New York, 2014, pp. 6155–6160. https://doi.org/10.1109/CDC.2014.7040353

[14] Sreenath, K., Michael, N., and Kumar, V., "Trajectory Generation and Control of a Quadrotor with a Cable-Suspended Load-A Differentially-Flat Hybrid System," *2013 IEEE International Conference on Robotics and Automation (ICRA)*, Inst. of Electrical and Electronics Engineers, New York, 2013, pp. 4888–4895. https://doi.org/10.1109/ICRA.2013.6631275

[15] Sreenath, K., Lee, T., and Kumar, V., "Geometric Control and Differential Flatness of a Quadrotor UAV with a Cable-Suspended Load," *52nd IEEE Conference on Decision and Control*, Inst. of Electrical and Electronics Engineers, New York, 2013, pp. 2269–2274. https://doi.org/10.1109/CDC.2013.6760219

[16] Dhiman, K. K., Kothari, M., and Abhishek, A., "Autonomous Load Control and Transportation Using Multiple Quadrotors," *Journal of Aerospace Information Systems*, Vol. 17, No. 8, 2020, pp. 1–19.

[17] Rastgoftar, H., and Atkins, E. M., "Cooperative Aerial Lift and Manipulation (CALM)," *Aerospace Science and Technology*, Vol. 82, 2018, pp. 105–118. https://doi.org/10.1016/j.ast.2018.09.005

[18] Meissen, C., Klausen, K., Arcak, M., Fossen, T. I., and Packard, A., "Passivity-Based Formation Control for UAVs with a Suspended Load," *IFAC-PapersOnLine*, Vol. 50, No. 1, 2017, pp. 13,150–13,155. https://doi.org/10.1016/j.ifacol.2017.08.2169

[19] Gassner, M., Cieslewski, T., and Scaramuzza, D., "Dynamic Collaboration Without Communication: Vision-Based Cable-Suspended Load Transport with Two Quadrotors," *2017 IEEE International Conference on Robotics and Automation (ICRA)*, Inst. of Electrical and Electronics Engineers, New York, 2017, pp. 5196–5202.

[20] Berrios, M. G., Tischler, M. B., Cicolani, L. S., and Powell, J. D., "Stability, Control, and Simulation of a Dual Lift System Using Autonomous r-max Helicopters," *70th American Helicopter Society*, Vol. 3, American Helicopter Soc. (AHS) International, Jan. 2014, pp. 2195–2213.

[21] Michael, N., Fink, J., and Kumar, V., "Cooperative Manipulation and Transportation with Aerial Robots," *Autonomous Robots*, Vol. 30, No. 1, 2011, pp. 73–86.

[22] Goodarzi, F. A., and Lee, T., "Stabilization of a Rigid Body Payload with Multiple Cooperative Quadrotors," arXiv preprint arXiv:1511.02180, 2015, http://arxiv.org/abs/1511.02180. https://doi.org/10.1115/1.4033945

[23] Wu, G., and Sreenath, K., "Geometric Control of Multiple Quadrotors Transporting a Rigid-Body Load," *53rd IEEE Conference on Decision and Control*, Inst. of Electrical and Electronics Engineers, New York, 2014, pp. 6141–6148.

[24] Lee, T., "Geometric Control of Quadrotor UAVs Transporting a Cable-Suspended Rigid Body," *IEEE Transactions on Control Systems Technology*, Vol. 26, No. 1, 2017, pp. 255–264.

[25] Nair, S. H., Banavar, R. N., and Maithripala, D. H. S., "Control Synthesis for an Underactuated Cable Suspended System Using Dynamic Decoupling," *2019 American Control Conference (ACC)*, Inst. of Electrical and Electronics Engineers, New York, 2019, pp. 2645–2650.

[26] Kotaru, P., Wu, G., and Sreenath, K., "Differential-Flatness and Control of Quadrotor (s) with a Payload Suspended Through Flexible Cable (s)," *Indian Control Conference (ICC)*, Inst. of Electrical and Electronics Engineers, New York, 2018, pp. 352–357. https://doi.org/10.1109/INDIANCC.2018.8308004

[27] Xu, R., and Özgüner, Ü., "Sliding Mode Control of a Class of Underactuated Systems," *Automatica*, Vol. 44, No. 1, 2008, pp. 233–241, http://linkinghub.elsevier.com/retrieve/pii/S0005109807002713. https://doi.org/10.1016/j.automatica.2007.05.014

[28] Zhu, B., Zhang, Q., and Liu, H. H.-T., "A Comparative Study of Robust Attitude Synchronization Controllers for Multiple 3-DOF Helicopters," *American Control Conference (ACC)*, Inst. of Electrical and Electronics Engineers, New York, 2015, pp. 5960–5965.

[29] Gernot, H., "A Simulative Study on Active Disturbance Rejection Control (ADRC) as a Control Tool for Practitioners," *Electronics*, Vol. 2, No. 4, 2013, pp. 246–279.

[30] Roza, A., and Maggiore, M., "A Class of Position Controllers for Underactuated VTOL Vehicles," *IEEE Transactions on Automatic Control*, Vol. 59, No. 9, 2014, pp. 2580–2585. https://doi.org/10.1109/TAC.2014.2308609

[31] Qian, L., "Path Following Control for Multiple Quadrotors Carrying a Rigid-Body Slung Payload," Ph.D. Thesis, Univ. of Toronto, Toronto, March 2021, https://hdl.handle.net/1807/104991.

[32] Deshpande, V. S., and Phadke, S. B., "Control of Uncertain Nonlinear Systems Using an Uncertainty and Disturbance Estimator," *Journal of Dynamic Systems, Measurement, and Control*, Vol. 134, No. 2, 2012, p. 24501.

[33] El-Hawwary, M. I., and Maggiore, M., "Reduction Theorems for Stability of Closed Sets with Application to Backstepping Control Design," *Automatica*, Vol. 49, No. 1, 2013, pp. 214–222.